Simulation of Precipitate Evolution in Fe-Based Alloys

V. V. Popov

Abstract In this chapter possibilities of simulation of precipitate evolution in Fe-based alloys are analyzed. At first separate stages of the process are considered: growth, dissolution and coarsening, and then possibilities of simulation of all the stages of evolution including nucleation in the framework of a unified approach are analyzed. The results obtained are generalized on a case of simulation of precipitate evolution in multicomponent systems. The results of numerical calculations are compared to the available experimental data. Most of examples are concerned with simulation of carbides, nitrides and carbonitride behavior at heat treatment of steels. In the concluding section of the chapter the analysis of possibilities of simulation of precipitate evolution in Fe-based alloys is summed up, and the problems retarding practical kinetic calculations in real commercial alloys are formulated.

Keywords Simulation · Numerical methods · Steels · Carbonitrides · Dissolution · Nucleation · Coarsening

1 Introduction

The second phase particles present in metal alloys can strongly affect their structure and properties, this influence being both beneficial, and adverse. Heat treatment of alloys, containing dispersed particles, should ensure such morphology, sizes and volume fraction of precipitates which provide an optimal complex of mechanical properties. In the development of precipitation hardening and ageing alloys numerous experimental studies have been carried out on the

V. V. Popov (✉)
Institute of Metal Physics, Ural Branch, Russian Academy of Sciences,
S. Kovalevskaya Street, 18, Ekaterinburg, Russia 620990,
e-mail: vpopov@imp.uran.ru

precipitates behavior at heat treatment, because without such investigations it was impossible to find a reasonable approach to the choice of alloys compositions and regimes of their heat treatment. Such studies are quite expensive and laborious, but it has been impossible to do without them till recently. The situation has considerably changed in the last years. The creation of powerful high-productive computers and decreasing deficiency of thermodynamic and diffusion data promoted an appearance of publications devoted to simulation of precipitates behavior in metal alloys. In the present paper possibilities of analytical description and simulation of precipitate evolution in metal alloys at heat treatment are analyzed by an example of Fe-based alloys. Successful simulation of evolution of structure of steels and alloys at various processes became possible recently due to high-productive computer technologies, and publications on this problem appear constantly (see, e.g., [1–8]).

In this chapter the methods of simulation of precipitates evolution in steels at isothermal annealing are considered. The main goal of this simulation is to find temporal dependence of the parameters characterizing precipitate ensemble.

The problem of precipitate evolution in an alloy corresponds to the problems of diffusion in areas with moving boundaries; it is the so-called Stephan problem [9]. At present it is not possible to solve this problem in a general form, not only by analytical, but even by numerical methods. From mathematical point of view, the boundary-value problems of diffusion for areas with moving boundaries differ principally from classical problems. The main difficulty in the solution of such problems is that the mass balance conditions at interfaces refer them to the type of non-linear problems, that is, to the problems with non-linear boundary conditions, even in case of constant diffusion coefficients. That is why, as a rule, only some particular cases are considered, using numerous simplifications and assumptions. In particular, only binary systems were mainly considered so far, for which it is much easier to obtain an analytical solution and to carry out the simulation.

Considerable progress in working out methods of solving such problems has been achieved recently due to, first of all, the development of numerical simulation methods and increasing computer power. However, a number of simplifications must be still used in simulation for two main reasons. Firstly, it is the insufficient development of the numerical methods of solving such problems, and secondly, the absence of the data on some parameters required for calculations.

We suppose that the local thermodynamic equilibrium is established at interfaces, the phase composition of the diffusion zone corresponds to the equilibrium, and the kinetics of the process is purely diffusional. Thus, it is assumed that the velocity of phase transformation at an interface is much higher than the diffusion. For the systems considered such an assumption is confirmed by a number of experimental results [10]. It is used in most of papers dealing with simulation of precipitate evolution in metal alloys, and Hillert and Agren [11] showed that calculations based on this assumption are valid even at low temperatures, when the alloying elements have the reduced mobility.

In the present chapter only the cases when the precipitate evolution is controlled by volume diffusion are considered, though it is known that this process may be

controlled by other mechanisms of mass transfer, such as, for example, dislocation diffusion or grain-boundary diffusion. However, for these cases it is, as a rule, not possible to carry out practical calculations, because of the lack of data on the values of the required parameters. Besides, in this chapter the main attention is paid to precipitates evolution in austenite at such temperatures when the mass transfer by volume diffusion is dominating.

Generally speaking, the morphology of particles must be determined as a part of the problem solution, but in this case the problem cannot be solved analytically, and that is why in most cases the particle shape is given a priori and as a rule it is chosen as spherical, and in further consideration this very assumption will be used.

As a rule, precipitates growth, dissolution and coarsening are considered as different processes, though in essence they are particular cases of one and the same process of evolution of precipitates ensemble. Separate consideration of growth, dissolution and coarsening is convenient, because the moving forces of these processes are different constituents of the free energy. In the cases of growth or dissolution it is, first of all, the chemical free energy, whereas in case of coarsening it is the surface free energy.

In further sections of the present chapter an attempt is undertaken to describe as generally as possible the evolution of precipitates in steels.

2 Simulation of Precipitates Growth and Dissolution

In case of precipitates growth and dissolution in a metal matrix the process is mainly controlled by the system tendency to decrease its chemical free energy, which is realized through variations of the volume fraction of precipitates and concentrations of components in the matrix.

Dependently on the chemical composition of precipitates and matrix, as well as on the process temperature, an interface can shift both towards the solid solution (particle growth) and towards the particle (its dissolution) due to the reaction diffusion. Besides, the new phase layers may appear in the diffusion zone with their further growth at an expense of the initial constituents of the system. Generally speaking, considering precipitates growth and dissolution one should take into account the polydispersity of precipitates ensemble and the effect of particle sizes on equilibrium conditions at interfaces, but it is commonly assumed that at the stages of growth and dissolution the particle size distribution (PSD) affects only slightly, and its effect may be neglected. It is not always so, but at first we assume that all the particles are of the same shape and sizes, and the influence of the interface curvature on the local equilibrium conditions is not taken into account. We shall restrict our consideration to a one-dimensional case (for a spherical symmetry), as it enables to take into account the main features of the process of precipitates diffusion interaction with a matrix without an excess complication of the problem.

Fig. 1 Concentration
distribution of a solute in a
spherical particle surrounding
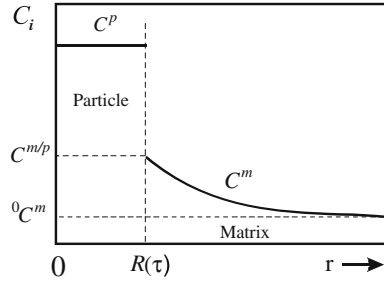
2.1 Methods of Simulation of Precipitates Growth and Dissolution

The simplest description corresponds to the growth or dissolution of precipitates of constant composition in binary systems. In this case one should not take into account interaction of components in a solid solution at diffusion, and the component concentrations at interfaces are constant, and their values can be determined directly from the corresponding phase diagrams. Most of the available analytical solutions correspond to this very case. As applied to the growth and dissolution of carbides and nitrides in steels, these solutions may be used, with certain reservations, only for the case of Fe carbides growth and dissolution in carbon steels.

In the first studies of precipitate growth and dissolution, which are reviewed in [12], the growth and dissolution of one precipitate of constant composition in an infinite matrix of a binary alloy was considered, the diffusion coefficient being assumed constant. The scheme of concentration distribution of a solute in a particle surrounding is shown in Fig. 1, where C^p and C^m are the solute concentrations in the particle and matrix, respectively; $^0C^m$ is the initial concentration in the matrix; $C^{m/p}$ is the concentration in the matrix at an interface with the particle; and R is the particle radius. This case corresponds to an infinitely small volume fraction of precipitates.

Taking into account the spherical symmetry of the problem, the diffusion equation in this case has the form:

$$\frac{\partial C^m}{\partial t} = D^m \frac{1}{r^2} \frac{\partial}{\partial r}\left(r^2 \frac{\partial C^m}{\partial r}\right) \tag{1}$$

where D^m is the solute diffusivity in the matrix.

The mass balance condition at an interface, determining its velocity, is expressed as:

$$\left(\frac{C^p}{v_a^p} - \frac{C^{m/p}}{v_a^m}\right)\frac{dR}{dt} = \frac{1}{v_a^m} D^m \frac{\partial C^m}{\partial r}\bigg|_{r=R} \tag{2}$$

where v_a^f is the volume per one atom of phase f.

Initial and boundary conditions for this case are:

$$R(t = 0) = R_0; \tag{3}$$

$$C^m(t = 0, R > R_0) = {}^{\circ}C^m; \tag{4}$$

$$C^m(t > 0, r = R) = C^{m/p}; \tag{5}$$

$$C^m(t > 0, r = \infty) = {}^{\circ}C^m \tag{6}$$

The boundary condition (5) serves as the local equilibrium condition, and it gives the equilibrium concentration at an interface which can be determined from the state diagram (in this case the correction on the interface curvature is not made).

The problem (1–6) was analyzed in [12], and the authors failed to find an exact analytical solution for non-zero initial radius. Three approximations were analyzed, namely, of linear gradient, stationary field and stationary interface. The linear gradient approximation assumes linear concentration profile in a matrix. According to [12], this approximation does not take into account the problem symmetry in the spherical case, which causes essential difficulties in the consideration of dissolution and makes it useless.

The stationary field approximation assumes that concentration field around the particle only slightly changes with time, and based on this assumption the left part of the diffusion equation is set equal to zero. As a result, the Laplace equation is obtained, the solution of which enables to find concentration distribution in the particle surrounding. Substitution of the as-determined concentration distribution into the mass balance equation gives the temporal dependence of precipitate sizes.

The immovable interface approximation assumes that the precipitate/matrix interface movement only slightly affects the concentration distribution in the particle surrounding, i.e., the concentration distribution is determined in the assumption that the interface is immovable. This enables to find an analytical expression for the solute concentration distribution in the matrix and analytical temporal dependence of precipitate sizes.

An exact analytical solution of the problem of a spherical precipitate dissolution in an infinite matrix was obtained in [13]. It should be noted, that the solution obtained is quite cumbersome and has a form of infinite series. However, comparing it with the solutions obtained based on various approximations, one can estimate correctness of the latter.

As demonstrated by an analysis carried out in [12, 14], the key parameter determining the validity of various approximations is the following one:

$$\lambda = \frac{C^{m/p} - {}^0C^m}{C^p - C^{m/p}}. \tag{7}$$

This analysis shows that the approximation of stationary interface is the best one at small $|\lambda|$. The results obtained using the stationary field approximation

Fig. 2 The scheme of matrix
partition into cells for
consideration of growth and
dissolution of diffusion
interacting particles [14]
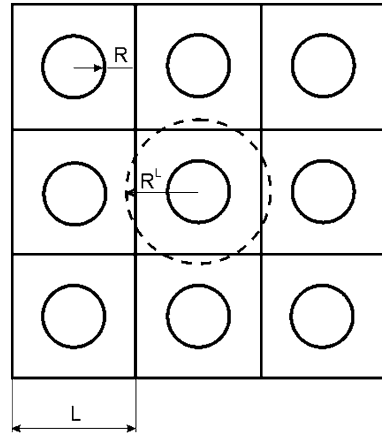
somewhat differ. However, with decreasing $|\lambda|$ the results of calculations made
with both approximations approach each other and the exact solution. At low $|\lambda|$ it
is quite correctly to use the stationary approximation.

In real steels a great number of second phase particles are always present, and if
their density is high, these particles are in diffusion interaction, because their
diffusion fields overlap, which affects the kinetics of their growth and dissolution.
To solve this problem the method is usually applied which enables to consider the
diffusion interaction of one particle with a matrix in a typical cell, limiting the
solid solution volume, and then to extend the regularities of the diffusion inter-
action in this volume on the whole totality of cells enclosing all matrix. All the
precipitates are assumed to have the same shape and sizes and to be uniformly
distributed in the matrix, i.e. the matrix is schematically divided into identical cells
with a particle in the center of each of them (Fig. 2). In this figure L is the distance
between particles, and R^L is the cell radius.

The problem symmetry imposes the condition of no diffusion flow through a
cell wall, i.e. the normal components of concentration gradients at the cell wall
must be zero. For mathematical simplification of the problem (reducing it to a one-
dimensional case) it is assumed that every particle is in the cell center, the sym-
metry of the cell being the same as that of the particle, and its volume being equal
to that of the cubic cell shown in Fig. 2. For example, in case of spherical particles
the cells also have the spherical shape, and their radius can be calculated as:

$$R^L = \left(\frac{3}{4\pi}\right)^{1/3} L = \left(\frac{3}{4\pi N_V}\right)^{1/3}, \tag{8}$$

where N_V is the number of particles in a unit volume.

Thus, the multi-particle diffusion problem is reduced to the one-particle one,
and the diffusion interaction in one cell is considered. Equations describing mass
transfer in the system, mass balance condition and local thermodynamic

equilibrium in this case are formulated as in the previous problem. The difference is only in the form of boundary conditions. The boundary conditions in this case instead of Eq. (6) include the following equation:

$$\left.\frac{\partial C^m}{\partial r}\right|_{r=R^L} = 0, \tag{9}$$

which expresses that the concentration gradient at a cell boundary equals to zero. These boundary conditions follow from the symmetry considerations and result from an assumption that all the particles have the same shape and size and are located at the same distances from each other.

The problems of growth and dissolution of precipitates in the limited matrix of binary systems were solved in [15–17], where quite cumbersome analytical solutions in form of infinite series were obtained. The analysis of the solutions obtained shows, that overlapping of the diffusion fields of different particles may appreciably affect the kinetics of precipitate growth and dissolution. This effect manifests itself in the fact that the velocities of precipitates growth or dissolution in the limited matrix decrease monotonically with time compared to those in an infinite matrix.

The solution of problems of precipitate growth and dissolution for multi-component systems is much more difficult than for binary, because of a number of factors. Firstly, to find concentration distributions in a particle surrounding one must solve not one differential equation, but a system of differential equations, because the flux of any component is determined not only by its concentration gradient, but by concentration gradients of all the alloy components. Secondly, unlike the case of binary systems, concentrations at interfaces are not known a priori, and to find them one must solve together with diffusion equations and mass balance equations the thermodynamic equations determining equilibrium conditions at interfaces. Thirdly, for multi-component systems diffusion coefficients commonly cannot be considered as constant. All these factors complicate the problem considerably.

That is why analytical solutions can be obtained only in the simplest cases, which are not quite adequate to the real processes in alloys at particle growth and/ or dissolution.

As a rule, in the available analytical solutions for multi-component systems the model of constant diffusion coefficients is used, and they correspond to the growth or dissolution of precipitates in an infinite matrix, because in this case it is easier to find concentration distributions of components, and concentrations at interfaces do not change with time [10, 18–21]. In [10, 19–21] the obtained analytical solutions were used for calculation of the diffusion interaction kinetics for a number of carbides in steels for the case of plane symmetry and semi-infinite matrix. The comparison of these calculations with experimental data obtained on diffusion couples demonstrated their good agreement, which shows that in some cases the analytical solutions can be applied to the description of diffusion interaction in multi-component systems as well. However, they may be used only for quite a limited category of problems.

In the last decades a number of studies appeared where such problem is solved using numerical methods. There are two reasons for using the latter. Firstly, the local equilibrium at a moving interface in a multi-component system cannot be determined directly from a common phase diagram. Secondly, the realistic consideration of diffusion in multi-component systems requires solution of a system of differential equations in partial derivatives, but not of one equation as in case of binary alloys. Besides, in general one must take into account the possibility of intermediate phase formation, changes in composition of an initial particle, concentration dependences of diffusion parameters, etc.

The problem definition in case of growth or dissolution of spherical precipitates in a limited matrix of $(N + 1)$-component alloy, in case when intermediate phase layers may form between the particle (phase 1) and matrix (phase Q), with allowance made for diffusion processes in particles, is as follows. We assume all the particles to have the same sizes and use the above-described approach based on the matrix partition into cells and consideration of the diffusion interaction in one cell. The scheme of concentration distribution of the i-th component in a cell for this case is shown in Fig. 3, where C_i^f is the i-th component concentration in phase f; $C_i^{f/f+1}$ is the i-th component concentration in phase f at an interface with $f + 1$; $R^{f/f+1}$ is the coordinate of an interface between f and $f + 1$.

Mathematical problem definition for this case is as follows. Mass transfer in every phase is described by N differential equations of the type:

$$\frac{\partial C_i^f}{\partial t} = \frac{1}{r^2}\frac{\partial}{\partial r}\left(r^2 \sum_{l=1}^{N} \widetilde{D}_{il}^f \frac{\partial C_l^f}{\partial r}\right), \tag{10}$$

where $\widetilde{D}_{il}^f$ are partial interdiffusion coefficients of components in phase f.
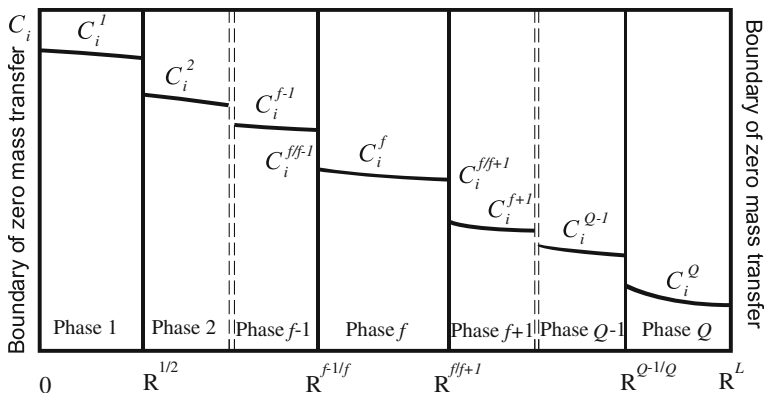

Fig. 3 The scheme of concentration distribution of the i-th component in a cell

The mass balance conditions include $(Q-1) \times N$ equations:

$$\left(\frac{C_i^{f+1/f}}{v_a^{f+1}} - \frac{C_i^{f/f+1}}{v_a^f} \right) \frac{dR_f}{dt} = \frac{1}{v_a^f} \sum_{l=1}^{N} \tilde{D}_{il}^f \frac{\partial C_l^f}{\partial r} \bigg|_{r=R_f} - \frac{1}{v_a^{f+1}} \sum_{l=1}^{N} \tilde{D}_{il}^{f+1} \frac{\partial C_l^{f+1}}{\partial r} \bigg|_{r=R_f},$$

(11)

Equilibrium conditions at interfaces include $(Q-1) \times (N+1)$ equations of the type

$$\overline{G}_i^{f/f+1} = \overline{G}_i^{f+1/f},$$

(12)

where $\overline{G}_i^{f/f+1}$ is the chemical potential of component i in phase f at an interface with $f+1$.

Initial conditions for this case include $Q-1$ equations of the type:

$$R^{f/(f+1)}(t=0) = R_0$$

(13)

and N equations

$$C_i^1(r < R_0, t = 0) = {}^0C_i^1$$

(14)

$$C_i^Q(r > R_0, t = 0) = {}^0C_i^Q,$$

(15)

where ${}^0C_i^1$ and ${}^0C_i^Q$ are initial concentrations of the i-th component in the precipitate and matrix.

Boundary conditions include N equations

$$\frac{\partial C_i^1}{\partial r} \bigg|_{r=0} = 0$$

(16)

$$\frac{\partial C_i^Q}{\partial r} \bigg|_{r=R^L} = 0,$$

(17)

which determine zero concentration gradients of components in a particle center and at a cell boundary.

For multi-component systems the solution of problems of precipitate growth and dissolution requires solving differential diffusion equations for every phase together with mass balance and thermodynamic equations determining mass balance conditions and local equilibrium at interfaces. Such problems can be solved only by numerical methods.

Application of numerical methods, such as finite differences, finite elements or boundary elements methods, almost does not require any simplifications and assumptions, which are usually needed for analytical methods.

The most widely used for the solution of diffusion problems is the finite differences method (or grid method), the main advantage of which is the simplicity of its numerical realization.

Differences methods are based on substitution of a region of continuous changing of arguments of the desired functions entered into differential equations for a grid with discrete set of points-nodes. The grid functions determined in discrete nodes are taken instead of continuous change of arguments, and the derivatives entering the differential equations and boundary conditions are substituted for difference relationships. As a result of such substitution, the boundary problem in partial derivatives is reduced to a system of algebraic difference equations referred to as finite-difference scheme.

When solving nonlinear parabolic differential diffusion equations, it is advisable to use conservative (divergent) implicit finite-difference schemes [22, 23]. An essential drawback of explicit finite-difference schemes compared to the implicit ones is the dependence of stability of the former on the relationship between time and space steps. As for the implicit scheme, it is absolutely stable at any ratios of steps, which enables to reduce the calculation time, though the explicit scheme simplifies the solution of the problem. Besides, an advantage of stable schemes is that it is not required to investigate additionally the velocity of the solution convergence, as it coincides with an order of approximation of a differential equation. An error inserted when a differential equation is substituted for a finite-difference scheme depends on the accuracy of derivatives approximation in the differential equation and boundary conditions.

Solution of nonstationary problems of diffusion and heat conductivity with movable interfaces, i.e. with changing regions of physical parameters continuity, requires working out special approaches. In the problems like Stephan's problem the main difficulty is that interfaces movement results in the appearance of new nodes of a spatial grid, which belonged to another phase, in one of the adjacent phases.

By now quite enough methods of overcoming difficulties of numerical calculations, caused by movable interfaces, have been worked out [24–35]. The available methods of solving problems like Stephan's problem are reviewed and analyzed in detail in [24, 25]. The drawback of most of these methods is that their application suggests the use of uniform spatial grids with one and the same space step in different phases, and in case of multi-component multi-phase problems this may require grids with the great number of spatial nodes. There is no such drawback in the method developed in [35, 36], in which its own spatial grid with the fixed number of nodes is introduced for every phase.

The position of phase transformation boundary coincides with a cell node. At phase transformations due to the change of phase sizes the grid step is changed in such way, that the number of nodes in every phase remains unchanged, and interphase boundaries coincide with the same grid nodes.

Application of the finite difference method to the solution of diffusion problems in case, when the formation of intermediate phase layers is possible, requires giving their finite thickness at an initial moment. Besides, at the initial moment the spatial grid and concentrations at every node for all the phases, including those absent in the diffusion zone at the initial moment, must be given. This would not
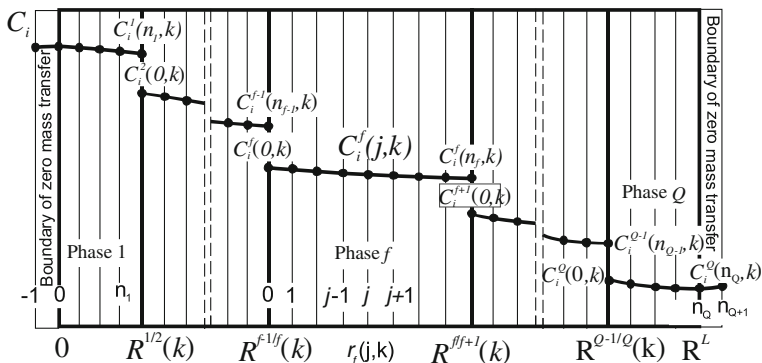
Fig. 4 Scheme of spatial partition and concentration distribution of the i-th component in a cell at the k-th time step

introduce a great error, if the thickness given at the initial moment is much lower than the finite phase thickness.

Let's consider the numerical solution of problem (10–17) by the finite difference method. The spatial partition was made in such way that for every phase its own spatial grid with the fixed number of nodes was introduced. Interphase boundaries coincided with the grid nodes, and the last node of phase f coincided with the zero node of phase $f + 1$. The allowance was made for the construction of non-uniform spatial grid. Figure 4 demonstrates the scheme of spatial partition and concentration distribution of the i-th component in a cell at the k-th time step, the following designations being used: $r_f(j, k)$ is the j-th node coordinate of phase f at the k-th time step; $R^{f/f+1}(k)$ is the position of phase boundary between f and $f + 1$ at the k-th time step; and $C_i^f(j, k)$ is the concentration of the i-th component in the j-th node of phase f at the k-th time step.

In the process of diffusion interaction every phase continuously changes its thickness, and coordinates of internal nodes of spatial grid change in such way that their distance from interphase boundaries always comprises a certain percent of the phase thickness. The internal nodes velocities are a linear combination of velocities of interfaces between the neighboring phases [35]:

$$V_f(r) = \frac{1}{R^{f/f+1} - R^{f-1/f}} \left\{ \left(R^{f/f+1} - r \right) \frac{dR^{f-1/f}}{dt} + \left(r - R^{f-1/f} \right) \frac{dR^{f/f+1}}{dt} \right\},$$

(18)

where $V_f(r)$ is the velocity of an internal point of phase f with r coordinate.

Intensity of concentration changes of components in a mobile point may be presented as follows (according to [36]):

$$\frac{dC_i^f}{dt} = \frac{\partial C_i^f}{\partial r} V_f(r) + \frac{\partial C_i^f}{\partial t}$$

(19)

Substitution of expressions (10) and (18) in this equation gives:

$$
\frac{\partial C_i^f}{\partial t} = \frac{\partial C_i^f}{\partial r} \cdot \frac{\left(R^{f/f+1} - r\right)\frac{\partial R^{f-1/f}}{\partial t} + \left(r - R^{f-1/f}\right)\frac{\partial R^{f/f+1}}{\partial t}}{R^{f/f+1} - R^{f-1/f}}
$$
$$
+ \frac{1}{r^2}\frac{\partial}{\partial r}\left(r^2 \sum_{l=1}^{N} \widetilde{D}_{il}\frac{\partial C_l^f}{\partial r}\right) \tag{20}
$$

The following designations are introduced: $\widetilde{D}_{il}^f(j \pm 1/2, k)$ are partial coefficients of interdiffusion in phase f corresponding to component concentrations median between their values in the j-th and the nearest to it nodes of phase f in the k-th time step; and $r_f(j \pm 1/2, k) = \left[r_f(j,k) + r_f(j \pm 1, k)\right]/2$ are coordinates of segment middles between the j-th and the nearest to it nodes of phase f in the k-th time step.

With these designations, the difference approximation of Eq. (20) may be written as follows, using the conservative absolutely stable implicit difference scheme:

$$
\frac{C_i^f(j, k+1) - C_i^f(j, k)}{t(k+1) - t(k)} = \frac{C_i^f(j+1, k+1) - C_i^f(j-1, k+1)}{r_f(j+1, k+1) - r_f(j-1, k+1)}
$$
$$
\times \frac{1}{R^{f/f+1}(k+1) - R^{f-1/f}(k+1)}
$$
$$
\times \left\{\left[R^{f/f+1}(k+1) - r_f(j, k+1)\right]\frac{R^{f-1/f}(k+1) - R^{f-1/f}(k)}{t(k+1) - t(k)}\right.
$$
$$
\left. + \left[r_f(j, k+1) - R^{f-1/f}(k+1)\right]\frac{R^{f/f+1}(k+1) - R^{f/f+1}(k)}{t(k+1) - t(k)}\right\}
$$
$$
+ \frac{1}{r_f^2(j, k+1)} \times \frac{2}{r_f(j+1, k+1) - r_f(j-1, k+1)}
$$
$$
\times \left[r_f^2(j+1/2, k+1)\sum_{l=1}^{N}\widetilde{D}_{il}^f(j+1/2, k+1)\frac{C_l^f(j+1, k+1) - C_l^f(j, k+1)}{r_f(j+1, k+1) - r_f(j, k+1)}\right.
$$
$$
\left. - r_f^2(j-1/2, k+1)\sum_{l=1}^{N}\widetilde{D}_{ij}^f(j-1/2, k+1)\frac{C_l^f(j, k+1) - C_l^f(j-1, k+1)}{r_f(j, k+1) - r_f(j-1, k+1)}\right] \tag{21}
$$

Using boundary conditions (16) and (17), one can write the difference approximation of differential Eq. (19) for the zero node of phase 1 and the n_Q-th node of phase Q as:

$$\frac{C_i^1(0, k+1) - C_i^1(0, k)}{t(k+1) - t(k)} = \frac{6}{r_1^2(1, k+1)}$$
$$\times \sum_{l=1}^{N} \tilde{D}_{il}^1(j/2, k+1) \cdot \left[C_l^1(1, k+1) - C_j^1(0, k+1)\right]$$

(22)

$$\frac{C_i^Q(n_Q, k+1) - C_i^Q(n_Q, k)}{t(k+1) - t(k)} = \frac{r_Q^2(n_Q - 1/2, k+1)}{(R^L)^2[R^L - r_Q(n_Q - 1, k+1)]^2} \times \sum_{l=1}^{N} \tilde{D}_{il}^Q(n_Q$$
$$- 1/2, k+1)$$
$$\cdot \left[C_l^Q(n_Q - 1, k+1) - C_l^Q(n_Q, k+1)\right]$$

(23)

As the boundary concentrations are the concentrations in the zero and the n_f-th nodes of the spatial grid, the difference approximation of balance Eq. (11) can be written as:

$$\left[\frac{C_i^{f+1}(0, k+1)}{v_a^{f+1}} - \frac{C_i^f(n_f, k+1)}{v_a^f}\right] \frac{R^{f/f+1}(k+1) - R^{f/f+1}(k)}{t(k+1) - t(k)}$$
$$= \frac{1}{v_a^f} \sum_{l=1}^{N} \tilde{D}_{il}^f(1/2, k+1) \frac{C_l^f(n_f, k+1) - C_l^f(n_f - 1, k+1)}{R^{f/f+1}(k+1) - r_f(n_f - 1, k+1)}$$

(24)

$$- \frac{1}{v_a^{f+1}} \sum_{l=1}^{N} \tilde{D}_{il}^{f+1}(1/2, k+1) \frac{C_l^{f+1}(1, k+1) - C_l^{f+1}(0, k+1)}{r_{f+1}(1, k+1) - R^{f+1/f}(k+1)},$$

and the local thermodynamic equilibrium conditions at the $f/f+1$ interface are:

$$\overline{G}_i^{f/f+1}\left[C_1^f(n_f, k+1), \ldots, C_N^f(n_f, k+1)\right] = \overline{G}_i^{f+1/f}\left[C_1^{f+1}(0, k+1), \ldots, C_N^{f+1}(0, k+1)\right].$$

(25)

The most effective method of solving linear differential equations is the sweep method. However, in this case this method cannot be used directly, because the initial boundary problem was nonlinear, and hence the obtained system of finite-difference Eqs. (21–24) is also nonlinear. Besides, these nonlinear finite-difference equations must be solved together with transcendent thermodynamic Eq. (25), and this appreciably complicates the problem considered, because one must solve a system of transcendent equations of high dimensionality. To overcome this difficulty, an iteration procedure was used in [37], in which the whole system of equations was divided into several systems, and these systems were solved sequentially till the required accuracy was achieved. For every interface a system of thermodynamic and balance equations was solved, and then for every phase a system of difference diffusion equations was solved as well, and this procedure was repeated time and again.

We used an analogous procedure in [38], in simulation of kinetics of titanium carbide dissolution in austenite. This algorithm has a relatively slow convergence, and the solution accuracy is poorly controlled. That is why in [39, 40] we realized another approach, based on combined solution of diffusion equations, mass balance equations and thermodynamic equations.

Balance Eq. (24) contain interface coordinates, boundary concentrations and concentrations in the nodes nearest to boundaries as unknown parameters, i.e. they have the following form:

$$FB_i^f \Big[R^{f/f+1}(k+1), C_1^f\big(n_f-1, k+1\big), \ldots, C_N^f\big(n_f-1, k+1\big),$$
$$C_1^f(n_f, k+1), \ldots, C_N^f(n_f, k+1), C_1^{f+1}(0, k+1), \ldots, C_N^{f+1}(0, k+1), \qquad (26)$$
$$C_1^{f+1}(1, k+1), \ldots, C_N^{f+1}(1, k+1) \Big] = 0$$

Thermodynamic equations contain only the values of boundary concentrations as unknown parameters, and they are as follows:

$$FT_i^f \Big[C_1^f\big(n_f, k+1\big), \ldots, C_N^f\big(n_f, k+1\big), C_i^{f+1}(0, k+1), \ldots, C_N^{f+1}(0, k+1) \Big] = 0.$$
$$(27)$$

If concentrations the in nodes nearest to boundaries could be expressed explicitly by difference Eqs. (21–23) through the values of boundary concentrations and positions of interphase boundaries, and then substituted into balance Eq. (26), a system of not very high dimensionality would be obtained, consisting of balance and thermodynamic equations, the solution of which would give the values of boundary concentrations and positions of interphase boundaries at a new time step. Unfortunately, it is impossible to do so. However, in solving the problem by numerical methods it is quite enough that the relationship between concentrations in nodes nearest to the boundary, boundary concentrations and positions of interphase boundaries is implicitly given by (21–23), and we used this situation in working out the problem solution algorithm.

The step-by-step procedure was used in calculations, and based on the interphase boundary position and concentration distributions for the time t these parameters were calculated for $t + \Delta t$.

The calculation order was as follows:

1. A point of initial approximations for the values of boundary concentrations in every phase and position of interphase boundary at a new time step was chosen.
2. Points in the neighborhood of the point of initial approximations were given.
3. For the point of initial approximations and the points in its neighborhood concentration distributions in all phases were calculated. In every case the spatial grid was reconstructed taking into account the boundary shift at the transition to a new time step, and concentration distributions in the phases

present were found through the solution of the system of difference Eq. (21–23) by the sweep method. Iteration procedures together with the sweep method were used in solution of difference equations. The finite-difference equations were linearized, i.e. diffusion coefficients were substituted in them for concentrations taken in the previous iteration, and for the first iteration in the previous time step.

4. The value of functions FB_i^f and FT_i^f were calculated in the point of initial approximations and in the points in its neighborhood, for which the values of boundary concentrations and positions of interphase boundary were used, as well as the values of concentrations in the nodes nearest to the boundary, determined at the third step.

5. The values of the derivatives of functions FB_i^f and FT_i^f for boundary concentrations and interface coordinates in a point corresponding to the initial approximations were found by the numerical differentiation.

6. Corrections to the initial approximations and specified values of the unknowns were found by the Newton-Raffson method based on the determined values of FB_i^f and FT_i^f functions and their derivatives.

The data obtained in the cycle (2–6) were used as an initial approximation for the new iteration, i.e. the calculation was repeated from point 2. If the consequent iteration differed from the previous one by a value smaller than the given convergence accuracy, then the iteration exit was performed.

As mentioned above, in solving difference equations one must use iteration procedures together with the sweep method, i.e. solve systems of equations many times, because of concentration dependences of diffusion coefficients, which considerably increase the computation time. To accelerate the calculation procedure, in our further studies we used a parallel algorithm of matrix sweep, which was realized on a multi-processor computation complex [41].

2.2 Simulation of Carbides and Nitrides Growth and Dissolution in Austenite

Solutions of diffusion problems like Stephan's problem for multi-phase multi-component systems are concerned with difficulties caused not only by their complex numerical realization, but with the absence in many cases of the required data on various parameters. Very often it is for this reason that different simplifications are to be used, and one has to restrict consideration to a relatively small number of components.

By now, because of the deficiency of data on the diffusion parameters, it is actually impossible to carry out practical calculations of growth or dissolution of particles in the systems with more than three components.

Fig. 5 The scheme of spatial
partition and concentration
distributions of components
in a cell for a case of carbide
or nitride dissolution in steel
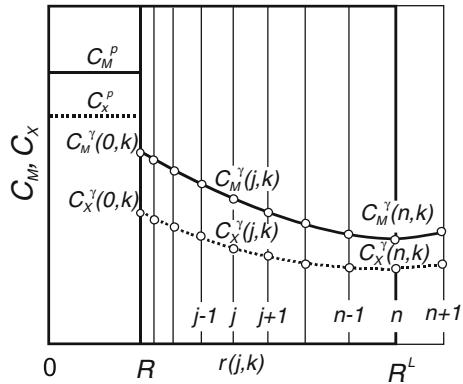
Let's consider application of the method described in the previous section for simulation of growth and dissolution of carbides and nitrides of constant composition, $Fe_zM_{(1-z)}X_n$, in the austenite of triple Fe-M-X systems (where M is a carbide- or nitride-forming element, and X is carbon or nitrogen). The scheme of concentration distribution and spatial grid construction in a cell for this case is shown in Fig. 5. The Fe-M-X systems can be considered as model relative to real steels. Analysis of the results of calculations of dissolution kinetics of carbides and nitrides in such systems may be helpful in the proper choice of heat treatment of steels.

Taking into account, that the diffusion mobility of interstitial elements is much higher than that of substitutional, a simplified method suggested in [22, 42] can be used for the description of interdiffusion in austenite. In this case the mass transfer in the system can be described by a system of equations:

$$\frac{\partial C_M^\gamma}{\partial t} = \frac{1}{r^2}\frac{\partial}{\partial r}\left(r^2 \widehat{D}_M^\gamma \frac{\partial C_M^\gamma}{\partial r}\right), \tag{28}$$

$$\frac{\partial C_X^\gamma}{\partial t} = \frac{1}{r^2}\frac{\partial}{\partial r}\left(r^2 \widetilde{D}_{XX}^\gamma \frac{\partial C_X^\gamma}{\partial r} + r^2 \widetilde{D}_{XM}^\gamma \frac{\partial C_M^\gamma}{\partial r}\right), \tag{29}$$

where indexes M and X denote, respectively, the carbide- or nitride-forming element and carbon or nitrogen; $\widehat{D}_M^\gamma$ is the effective coefficient of interdiffusion of substitutional element in the austenite of the triple system Fe-M-X.

Conditions at a cell boundary are:

$$\left.\frac{\partial C_M^\gamma}{\partial r}\right|_{r=R^L} = 0 \tag{30}$$

and

$$\left.\frac{\partial C_X^\gamma}{\partial r}\right|_{r=R^L} = 0 \tag{31}$$

Mass balance conditions at an interphase boundary are expressed by the equations:

$$\left(\frac{C_M^p}{v_a^p} - \frac{C_M^{\gamma/p}}{v_a^\gamma} \right) \frac{dR}{dt} = \frac{1}{v_a^\gamma} \widehat{D}_M^\gamma \frac{\partial C_M^\gamma}{\partial r}\bigg|_{r=R} \tag{32}$$

and

$$\left(\frac{C_X^p}{v_a^p} - \frac{C_X^{\gamma/p}}{v_a^\gamma} \right) \frac{dR}{dt} = \frac{1}{v_a^\gamma} \left(\widetilde{D}_{XX}^\gamma \frac{\partial C_X^\gamma}{\partial r}\bigg|_{r=R} + \widetilde{D}_{XM}^\gamma \frac{\partial C_M^\gamma}{\partial r}\bigg|_{r=R} \right). \tag{33}$$

Taking into account the constant composition of interstitial phase $M_zFe_{(1-z)}X_n$, the local thermodynamic equilibrium conditions at the interphase boundary take the form:

$$z\overline{G}_M^{\gamma/p} + (1 - z)\overline{G}_{Fe}^{\gamma/p} + n\overline{G}_X^{\gamma/p} = G_{M_zFe_{1-z}X_n}, \tag{34}$$

where $G_{M_zFe_{1-z}X_n}$ is the Gibbs energy of one $M_zFe_{1-z}X_n$ formula unit.

For sparingly soluble carbides and nitrides of MX_n type the equilibrium conditions can be expressed by solubility products of these compounds in austenite.

Equations (19), describing concentration changes of components in mobile nodes, taking into account expressions (18) and (28–29), in this case take the form:

$$\frac{\partial C_M^\gamma}{\partial t} = \frac{\partial C_M^\gamma}{\partial r} \left[\frac{R^L - r}{R^L - R} \frac{dR}{dt} \right] + \frac{1}{r^2} \frac{\partial}{\partial r} \left[r^2 \widehat{D}_M^\gamma \frac{\partial C_M^\gamma}{\partial r} \right] \tag{35}$$

and

$$\frac{\partial C_X^\gamma}{\partial t} = \frac{\partial C_X^\gamma}{\partial r} \left[\frac{R^L - r}{R^L - R} \frac{dR}{dt} \right] + \frac{1}{r^2} \frac{\partial}{\partial r} \left[r^2 \left(\widetilde{D}_{XX}^\gamma \frac{\partial C_X^\gamma}{\partial r} + \widetilde{D}_{XM}^\gamma \frac{\partial C_M^\gamma}{\partial r} \right) \right]. \tag{36}$$

In the difference approximation Eq. (35–36) take the form:

$$\frac{C_M^\gamma(j,k+1) - C_M^\gamma(j,k)}{t(k+1) - t(k)} = \frac{C_M^\gamma(j+1,k+1) - C_M^\gamma(j-1,k+1)}{r(j+1,k+1) - r(j-1,k+1)} \times \frac{R^L - r(j,k+1)}{R^L - R(k+1)}$$

$$\times \frac{R(k+1) - R(k)}{t(k+1) - t(k)} + \frac{1}{r_f^2(j,k+1)} \times \frac{2}{r_f(j+1,k+1) - r_f(j-1,k+1)}$$

$$\times \left\{ \frac{r^2(j+1/2,k+1)}{r(j+1,k+1) - r(j,k+1)} \widehat{D}_M^\gamma(j+1/2,k+1) \left[C_M^\gamma(j+1,k+1) - C_j^f(j,k+1) \right] \right.$$

$$\left. - \frac{r^2(j-1/2,k+1)}{r(j,k+1) - r(j-1,k+1)} \widehat{D}_M^\gamma(j-1/2,k+1) \left[C_M^\gamma(j,k+1) - C_j^f(j-1,k+1) \right] \right\}$$

$$\tag{37}$$

$$\frac{C_X^{\gamma}(j, k+1) - C_X^f(j, k)}{t(k+1) - t(k)} = \frac{C_X^{\gamma}(j+1, k+1) - C_X^{\gamma}(j-1, k+1)}{r(j+1, k+1) - r(j-1, k+1)} \times \frac{R^L - r(j, k+1)}{R^L - R(k+1)}$$

$$\times \frac{R(k+1) - R(k)}{t(k+1) - t(k)} + \frac{1}{r_f^2(j, k+1)} \times \frac{2}{r_f(j+1, k+1) - r_f(j-1, k+1)}$$

$$\times \left\{ \frac{r^2(j+1/2, k+1)}{r(j+1, k+1) - r(j, k+1)} \left[\widetilde{D}_{XX}^{\gamma}(j+1/2, k+1)(C_X^{\gamma}(j+1, k+1) - C_X^{\gamma}(j, k+1)) \right. \right.$$

$$\left. + \widetilde{D}_{XM}^{\gamma}(j+1/2, k+1)(C_M^{\gamma}(j+1, k+1) - C_M^{\gamma}(j, k+1)) \right]$$

$$- \frac{r^2(j-1/2, k+1)}{r(j, k+1) - r(j-1, k+1)} \left[\widetilde{D}_{XX}^{\gamma}(j-1/2, k+1) \left(C_X^{\gamma}(j, k+1) - C_X^f(j-1, k+1) \right) \right.$$

$$\left. \left. + \widetilde{D}_{XM}^{\gamma}(j-1/2, k+1)(C_M^{\gamma}(j, k+1) - C_M^{\gamma}(j-1, k+1)) \right] \right\}$$

$$(38)$$

Based on the boundary conditions (30–31), the difference approximation for a node located at a cell boundary takes the form:

$$\frac{C_M^{\gamma}(n, k+1) - C_M^{\gamma}(n, k)}{t(k+1) - t(k)} = \frac{r^2(n-1/2, k+1)}{(R^L)^2 [R^L - r(n-1, k+1)]^2}$$

$$\times \widehat{D}_M^{\gamma}(n-1/2, k+1) \times [C_M^{\gamma}(n-1, k+1) - C_M^{\gamma}(n, k+1)] \qquad (39)$$

$$\frac{C_X^{\gamma}(n, k+1) - C_X^{\gamma}(n, k)}{t(k+1) - t(k)} = \frac{r^2(n-1/2, k+1)}{(R^L)^2 [R^L - r(n-1, k+1)]^2}$$

$$\times \left\{ \widetilde{D}_{XX}^{\gamma}(n-1/2, k+1) \times [C_X^{\gamma}(n-1, k+1) - C_X^{\gamma}(n, k+1)] \right. \qquad (40)$$

$$\left. + \widetilde{D}_{XM}^{\gamma}(n-1/2, k+1) \times [C_M^{\gamma}(n-1, k+1) - C_M^{\gamma}(n, k+1)] \right\}$$

The difference approximation of balance Eq. (32–33) can be written as:

$$\left(\frac{C_M^p}{\upsilon_a^p} - \frac{C_M^{\gamma}(0, k+1)}{\upsilon_a^{\gamma}} \right) \frac{R(k+1) - R(k)}{t(k+1) - t(k)}$$

$$= \frac{1}{\upsilon_a^{\gamma}} \widehat{D}_M^{\gamma}(1/2, k+1) \frac{C_M^{\gamma}(1, k+1) - C_M^{\gamma}(0, k+1)}{r(1, k+1) - r(0, k+1)} \qquad (41)$$

$$\left(\frac{C_X^p}{\upsilon_a^p} - \frac{C_X^{\gamma}(0, k+1)}{\upsilon_a^{\gamma}} \right) \frac{R(k+1) - R(k)}{t(k+1) - t(k)}$$

$$= \frac{1}{\upsilon_a^{\gamma}} \left\{ \widetilde{D}_{XX}^{\gamma}(1/2, k+1) \frac{C_X^{\gamma}(1, k+1) - C_X^{\gamma}(0, k+1)}{r(1, k+1) - r(0, k+1)} \right. \qquad (42)$$

$$\left. + \widetilde{D}_{XM}^{\gamma}(1/2, k+1) \frac{C_M^{\gamma}(1, k+1) - C_M^{\gamma}(0, k+1)}{r(1, k+1) - r(0, k+1)} \right\}$$

Using the grid variables, Eq. (34), expressing conditions of local thermodynamic equilibrium at an interphase boundary, takes the form:

$$z\overline{G}_M^{\gamma}[C_M^{\gamma}(0,k+1), C_X^{\gamma}(0,k+1)]$$
$$+ (1-z)\overline{G}_{Fe}^{\gamma}[C_M^{\gamma}(0,k+1), C_X^{\gamma}(0,k+1)] \tag{43}$$
$$n\overline{G}_X^{\gamma}[C_M^{\gamma}(0,k+1), C_X^{\gamma}(0,k+1)] = G_{M_z Fe_{1-z} X_n}$$

The system of Eqs. (37–43) relates the interphase boundary position to the concentration distribution at the previous and consequent time s, i.e. it describes the system evolution with time.

The calculations were done using the algorithm described in the previous section. In [10, 39, 40, 43] we carried out calculations of dissolution kinetics of carbides and nitrides in austenite, analyzed factors affecting their dissolution kinetics, and constructed kinetic nomograms for determination of the degree of dissolution of some carbides and nitrides in austenite. In these calculations it was assumed that at the initial moment the maximal possible amount of an excess phase is present in the steel of corresponding composition.

Dissolution of precipitates in multi-component systems differs from that in binary systems because in the former the dissolution kinetics is determined by the diffusion of atoms of several elements. Relationships between the diffusion mobility of components, the character of their interaction and compositions of the dissolving phase and matrix determine the values of boundary concentrations and concentration distributions of components in the matrix. In case of the limited matrix, diffusion fields of different precipitates may overlap, and due to different diffusion mobility of components the overlapping for different elements occurs at different steps of the process.

At carbides and nitrides dissolution simultaneous diffusion of metal elements and interstitials occurs. Diffusion coefficients of carbide- and nitride-forming elements are approximately by a factor of 4 lower than those of carbon and nitrogen. That is why the particle dissolution velocity is determined first of all by the diffusion mobility of atoms of slowly diffusing carbide- or nitride-forming element. The velocity of diffusion of interstitial atoms and the character of their interaction with the atoms of carbide- or nitride-forming element determine the value of the metal atom boundary concentration, which in its turn determines its concentration gradient in the matrix at an interface with the particle, the flux from the particle into the matrix and the velocity of dissolution. Besides, one should keep in mind that in most cases the carbon concentration increase in solid solution results in higher diffusion mobility of metal atoms [10].

As demonstrated by the analysis carried out in [40], the diffusion fields overlapping may cause considerable slowing of dissolution process. Overlapping of the diffusion fields of interstitial elements is achieved at the very first stages of the process, whereas their overlapping for the carbonitride-forming element is much less probable and is possible only at the late stages of dissolution process. The effect of overlapping of the interstitial element diffusion fields is the stronger the greater is its concentration change in the matrix. The effect of overlapping for the carbonitride-forming element is the more considerable the closer is the steel composition to the maximal solubility of interstitial phase.

Fig. 6 Effect of spherical
particle sizes of η-carbide
Fe3W3C on their dissolution
kinetics in a steel with
0.5 % C and 13 % W at
13,000 C
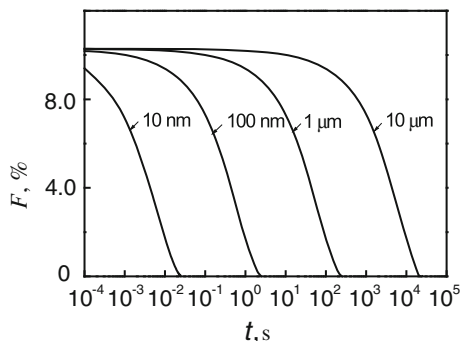
Kinetics of precipitates dissolution to a great extent depends on their initial size. It is known [44], that when precipitates dissolve in infinite matrix, the degree of their dissolution is determined by the value of t/R_0^2, i.e. the time required for the achievement of a certain degree of dissolution is proportional to their square radius. In case of the limited matrix the proportionality of time needed for the achievement of certain degree of precipitates dissolution to their square radius is not obvious, because the change of precipitates initial radius along with their constant volume fraction results in the change of distances between particles, i.e. of cell size. That is why calculations of dissolution kinetics of spherical particles of different radii in steels of one and the same chemical composition were carried out. The results of calculations for spherical particles of η-carbide Fe$_3$W$_3$C are shown in Fig. 6, which demonstrates temporal dependences of the volume fraction of precipitates (F). It is seen, that when precipitates dissolve in the limited matrix, the time required for an achievement of the given dissolution degree is proportional to their initial radius, as in case of infinite matrix. This proportionality is valid in a wide range of particle sizes and is observed even at a relatively high volume fraction of precipitates.

Based on the results of calculations, kinetic nomograms were constructed, which make possible to determine the degree of carbides and nitrides dissolution in steels of various compositions after different times of holding at various temperatures. These nomograms represent temporal dependences of volume fractions of corresponding phases. As mentioned above, it was assumed that in the initial state the maximal possible amount of the appropriate carbide or nitride phase is formed. The nomograms were constructed only for one initial radius of precipitates (1 μm), because the time required for an achievement of an appropriate degree of precipitates dissolution is proportional to their square radius, and hence these nomograms can be used for any initial particle size. Examples of such nomograms for VC$_{0.88}$, NbC, TiC, VN and NbN are given in Figs. 7, 8, 9, 10, 11.

Calculations of dissolution kinetics of carbides and nitrides of group IV–V elements were carried out for typical compositions of constructional steels (0.1 wt. % V, 0.05 wt. % Nb, 0.05 wt. % Ti, 0.05–0.5 wt. % C, and 0.01–0.03 wt. % N).
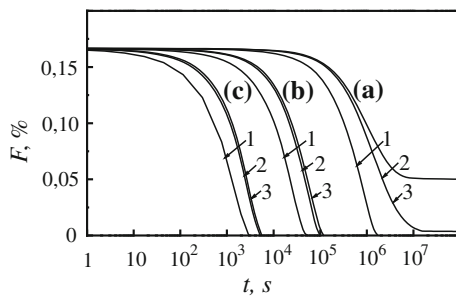
Fig. 7 Nomogram for determination of $VC_{0.88}$ dissolution degree at austenization of steels with 0.1 wt. % V and 0.1 (*1*), 0.3 (*2*) and 0.5 wt % C (*3*) at 900 (*a*), 1,000 (*b*) and 1,100 °C (*c*)
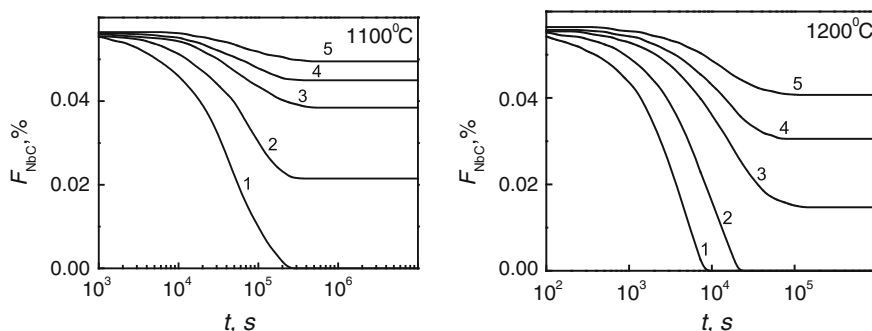

Fig. 8 Nomograms for determination of NbC dissolution degree at austenization at various temperatures of steels with 0.05 wt % Nb and various carbon content: *1*–0.05; *2*–0.1; *3*–0.2; *4*–0.3; *5*–0.5 wt % C
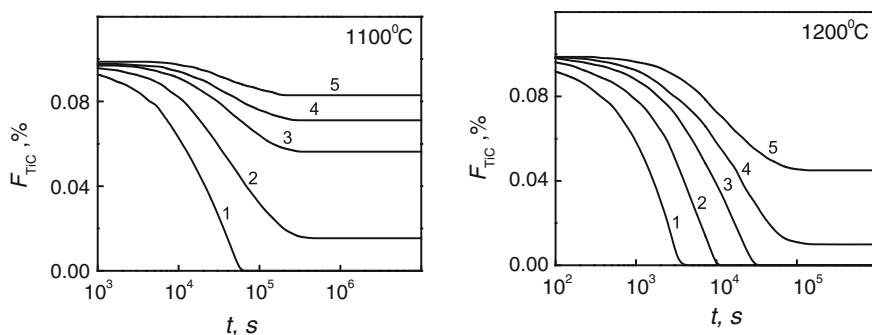

Fig. 9 Nomograms for determination of TiC dissolution degree at austenization at various temperatures of steels with 0.05 wt % Ti and various carbon content: *1*–0.05; *2*–0.1; *3*–0.2; *4*–0.3; *5*–0.5 wt % C

Fig. 10 Nomograms for determination of VN dissolution degree at austenizatioun at various temperatures of steels with 0.1 wt. % V and various nitrogen content: *1*–0.01; *2*–0.02; *3*–0.03 wt. % N
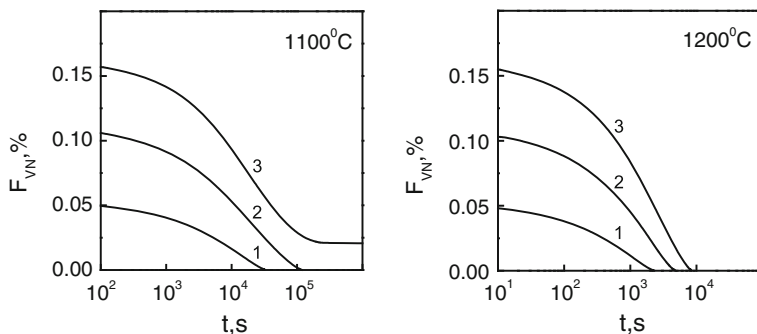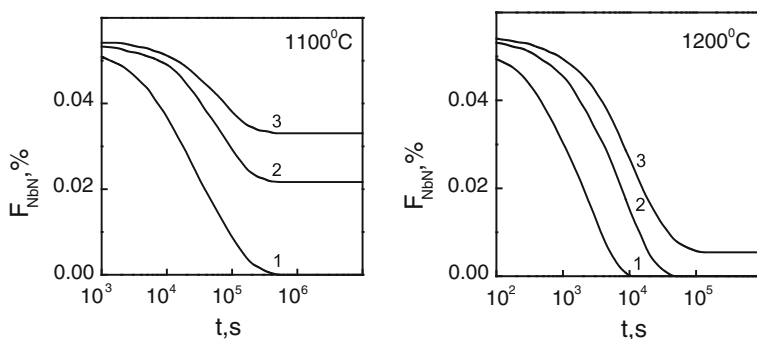

Fig. 11 Nomograms for determination of NbN dissolution degree at austenization at various temperatures of steels with 0.05 wt. % Nb and various nitrogen content: *1*–0.01; *2*–0.02; *3*–0.03 wt. % N

Using the nomograms shown in Figs. 7, 8, 9, 10, 11, one can determine the degree of dissolution of carbides and nitrides at austenization during the given time, the time required for an achievement of a given degree of their dissolution and the time of their complete dissolution, but one must know the average particle size in the initial state. As an example, let's determine the degree of niobium carbides dissolution in steel with 0.05 wt. % Nb and 0.1 wt. % C at 1,100 °C after isothermal annealing for 3,600 s, if the initial average size of the carbides was 200 nm. Let's use the nomogram in Fig. 8 (curve 2 for 1,100 °C). It was constructed for the initial size of 1 μm, whereas in the steel under consideration their size is 5 times smaller. It means that the time required for an achievement of a certain degree of dissolution is 25 times shorter than that according to the nomogram. Hence, we must determine from the nomogram the degree of carbides dissolution during 3,600 × 25 = 90,000 s. For this time their volume fraction decreases from 0.056 д 0 0.033 %, i.e. 41 % of the carbide phase dissolves.

The nomograms shown in Figs. 7, 8, 9, 10, 11 enable to make some general conclusions on the kinetics of carbide and nitride dissolution in steels at austenization. The precipitate dissolution is the slower the higher is thermal stability of an interstitial phase. It is seen that vanadium carbides and nitrides dissolve considerably faster than that of niobium and titanium. It is because the element concentrations in a matrix at its interface with a precipitate is the lower the higher is the thermal stability of the dissolving phase. With increasing content of carbon and nitrogen in a steel carbides and nitrides dissolution slows down, which results from decreasing concentration of a carbonitride-forming element at an interface with a dissolving particle. At relatively low temperatures complete dissolution may not be achieved. In this case the dissolving phase thermodynamic stability and carbon and nitrogen content in the steel will determine the maximal achievable degree of dissolution and the time required for the establishment of equilibrium.

The rising of heating temperature considerably affects the kinetics of precipitate dissolution. In this case not only equilibrium conditions at interfaces are changed, but the diffusion coefficients of components in matrix are increased.

Using such nomograms, one can choose the heat treatment regime ensuring the given degree of dissolution of an exceed phase.

It should be noted that the effect of kinetic factors manifests itself mainly at relatively low austenization temperatures (lower than $\sim 1,000\ ^\circ\text{C}$). At higher temperatures precipitates with not too coarse sizes, as a rule, dissolve very quickly, and the degree of the second phase dissolution is determined by thermodynamic factors. However, if in the initial state very coarse particles have formed in a steel, or if a heat treatment connected with fast and short-time heating is used, then the degree of precipitates dissolution will depend on kinetic factors at higher temperatures as well.

2.3 Simulation of Diffusion Interaction of Carbonitrides of Varying Composition with Matrix

As mentioned above, the lack of parameters required for calculations is one the reasons for making various simplifications and assumptions in simulation of precipitates evolution. Particularly, almost in all the available models of precipitate evolution the constant precipitate composition is assumed.

However, in some cases precipitates composition changes in the process of their evolution. In particular, in steels doped with strong carbonitride-forming elements of groups IV-V, carbonitrides can be formed, the composition of which can change at heat treatment due to the diffusion processes in them [10].

Calculations of the diffusion interaction of carbonitride precipitates of variable composition in steels were made in [45, 46]. The main problem was the absence of information on diffusion parameters in carbonitrides. That is why in our

calculations instead of coefficients of tracer diffusion of C and N in carbonitrides we used coefficients of diffusion of carbon and nitrogen in carbides and nitrides, respectively.

Calculations of the diffusion interaction of Ti carbonitrides with steels were made in [45]. The coefficients of tracer diffusion of C and N in carbides and nitrides were calculated based on the data on their chemical diffusion [47, 48], according to the formulas by Anderson and Agren, relating coefficients of tracer and chemical diffusion [49]. It was demonstrated that at high temperatures and long holding the composition of coarse nitrides formed at crystallization of an ingot may change in the depth of up to several microns, which is in agreement with the available experimental data [50].

Calculations of vanadium carbonitrides evolution in steels with allowance made for the diffusion in particles were carried out in [46]. The coefficient of tracer diffusion of C in the carbide was taken from [51], and that of N in the nitride was calculated based on the data of its chemical diffusion from [52], according to the formulas given in [49].

To evaluate the effect of diffusion in particles on the kinetics of their diffusion interaction with a matrix, we calculated the dissolution kinetics of cubic vanadium carbonitrides V(C,N) of various initial compositions in the austenite of steel with 0.1 %C, 0.01 %N and 0.1 %V at 10,000 C. The calculations were done with and without the consideration of the diffusion processes in precipitates at their diffusion interaction with the matrix. The initial diameter of the precipitates was assumed to be 100 nm, and their volume fraction corresponded to the value of the complete vanadium bonding into the carbonitrides.

Figure 12 demonstrates dependences of the volume fraction of vanadium carbonitrides for different initial compositions on the annealing duration, calculated with an assumption of their constant initial composition and taking into account the probability of its changing in the process of dissolution. It is obvious, that variations of carbonitrides initial composition have a strong effect on their dissolution kinetics, if the possibility of composition modification is not taken into account.

On the contrary, if the diffusion processes in carbonitrides are taken into account, the differences in their initial phase composition are quickly enough smoothed. These results show that the conclusions made based on calculations without consideration for the diffusion processes in carbonitride phase may be wrong.

For example, calculations made with the account of diffusion processes in carbonitrides demonstrate, that independently on the initial composition of carbonitrides, the latter cannot be dissolved completely in the steel of this composition at 1,000 °C, and their amount after the annealing for 0.5–1 h is practically independent on their initial composition. On the contrary, calculations made without taking into account the carbonitride composition modification, predict strong dependence of the residual amount of carbonitride on its initial composition, and for a certain interval of the initial compositions one may even expect the complete dissolution of carbonitrides.
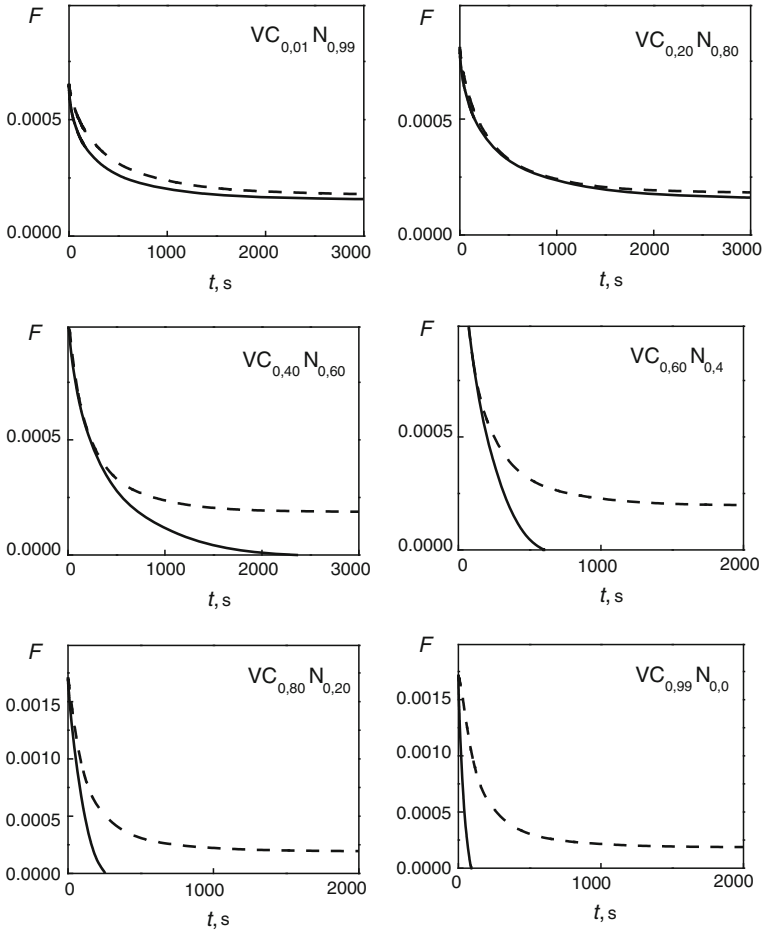
Fig. 12 Carbonitride volume fraction at 1,000 °C annealing of steel with 0.1 % C, 0.01 % N and 0.1 % V and with different initial compositions of carbonitride, calculated in the assumption of constant carbonitride composition (*solid lines*) and with consideration of its possible change at dissolution (*dashed lines*). The initial carbonitride composition is denoted in the figures

Figure 13 illustrates modification of concentration distribution in carbonitrides of different initial composition at annealing.

It is seen that distributions of C and N concentrations in carbonitrides intricately change at the diffusion annealing, because the character of the diffusion interaction is determined not only by the initial composition of carbonitrides, but also by the initial matrix composition and by the diffusion parameters of C and N in austenite and carbonitride. The local equilibrium establishes at carbonitride/austenite interface at the very beginning of the diffusion interaction. At further annealing modifications of boundary concentrations of carbon and nitrogen in carbonitride are not monotone. At first there is some enrichment of the carbonitride
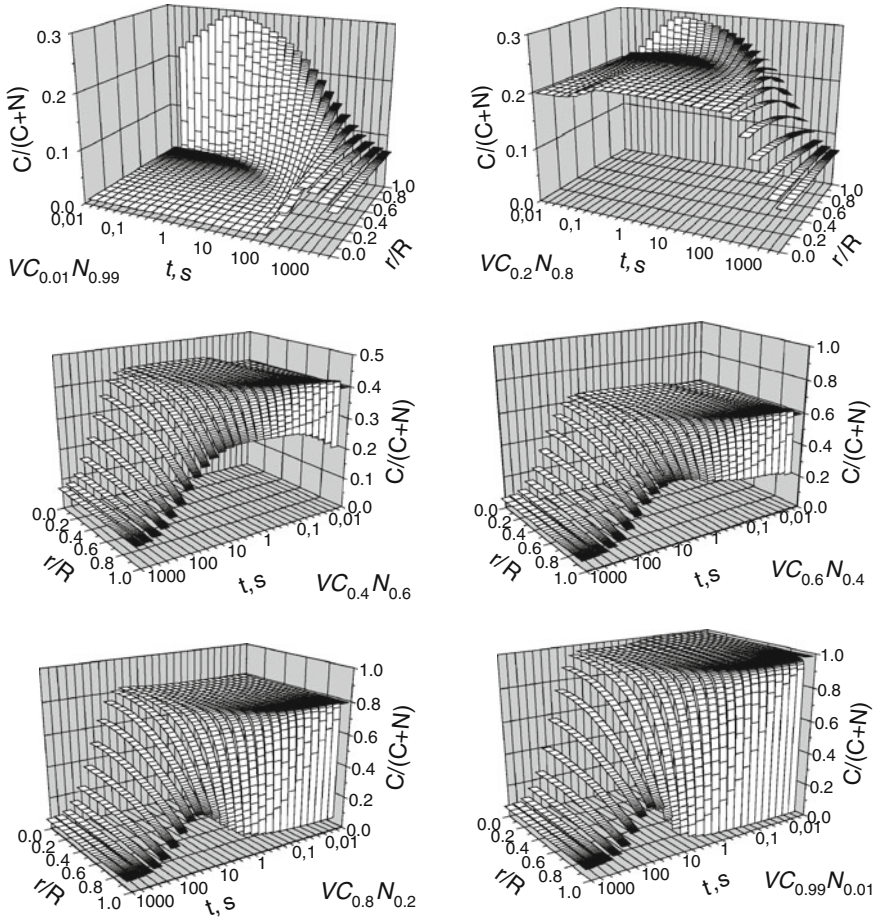
Fig. 13 Modification of vanadium carbonitrides composition at 1,000 °C annealing of steel with 0.1 % C, 0.01 % N and 0.1 % V and with different initial carbonitride compositions. The initial composition is written in the figures

near-boundary zone compared to the composition established at the initial moment, and this effect seems to be due to the relationship between the diffusion rates of C and N in carbonitride and austenite. At further diffusion interaction the phase composition approaches to the equilibrium, and the carbonitride composition evens out through the depth and approaches to the one and the same equilibrium composition, approximately corresponding to $VC_{0.07}N_{0.93}$.

The examples cited above show that in simulation of evolution of variable composition precipitates at heat treatment of metal alloys one must if possible take into account diffusion processes inside particles or at least estimate their effect on the kinetics of the process, as it appears to be quite significant.

3 Simulation of Particle Coarsening

When a two-phase alloy almost reaches the equilibrium phase composition through the processes of dissolution or growth, the stage of particle coarsening comes. By that moment the potentialities of decreasing of free energy volume constituent are practically exhausted, and the moving force for further evolution is the system's tendency to decrease its surface energy. It is realized through dissolution of fine particles and growth of coarse ones at practically unchanged volume fraction of the second phase. As a result, the area of interfaces reduces, and the free energy of the system diminishes, this process being referred to as Ostwald ripening, or particle coarsening. In this case there exists some critical radius R_c, at which the precipitate is in equilibrium with solid solution, and at $R > R_c$ it grows, whereas at $R < R_c$ it dissolves.

By now there have been published a lot of studies dealing with experimental investigations of particle coarsening, their theoretical treatment and numerical simulation of this process. The present study is not aimed at reviewing the available theories of Ostwald ripening and methods of its numerical simulation. We are going to touch mainly upon the problems which are of interest for the construction of a generalized model of precipitate evolution, which is considered in the next section, as well as of carbide and nitride precipitates coarsening.

The first theory of particle coarsening controlled by volume diffusion was developed by Lifshitz and Slezov [53], who considered a diluted binary alloy with infinitesimal volume fraction of second phase spherical particles distributed in a matrix. The problem definition is as follows. Mass transfer in a system is described by a stationary equation of diffusion for a spherical symmetry:

$$\frac{\partial}{\partial r}\left(r^2 \frac{\partial C^m}{\partial r}\right) = 0, \tag{44}$$

with the following boundary conditions

$$C^m(r = R) = C^{m/p}(R) \tag{45}$$

and

$$C^m(r = \infty) = \overline{C}^m. \tag{46}$$

Here $C^{m/p}(R)$ is a dissolved component concentration in a matrix at an interface with a particle of radius R, and $\overline{C}^m$ is an average concentration of the dissolved component in the matrix.

The use of the approximation of infinitesimal volume fraction excludes the possibility of overlapping diffusion fields of different precipitates, which makes easier to find concentration distributions in the areas surrounding particles.

It is assumed that the local equilibrium is established at all interfaces, and boundary concentrations are determined by the linearized form of Gibbs–Thomson equation:

$$C^{m/p}(R) = {}^eC^m + \frac{l^m}{R}, \tag{47}$$

where ${}^eC^m$ is the equilibrium concentration of the dissolved component in the matrix, and l^m is the matrix phase capillary length, which, according to [54], is equal to

$$l^m = \frac{2v_m^p \sigma\, {}^eC^m(1 - {}^eC^m)}{R_g T(C^p - {}^eC^m)}, \tag{48}$$

where v_m^p is the precipitate molar volume, σ is the specific surface energy, and R_g is the universal gas constant.

Velocities of interphase boundaries movement are determined by the mass balance Eq. (2).

Two more equations must be added to these ones. It is the equation of discontinuity in size space, describing evolution of the PSD function, $f(R,t)$:

$$\frac{\partial f}{\partial t} + \frac{\partial}{\partial R}\left(f\frac{dR}{dt}\right) = 0, \tag{49}$$

and the mass conservation condition:

$$\alpha_p C^p + \left(1 - \alpha_p\right)\overline{C}^m = C^{al}, \tag{50}$$

where α_p is the mole fraction of precipitating phase, and C^{al} is the dissolved component concentration in an alloy.

The distribution function is normalized by the number of particles per unit volume, N_V, that is

$$N_V = \int\limits_0^\infty f dR. \tag{51}$$

The mole fraction of precipitates is related to its volume fraction by an equation:

$$\alpha_p = \frac{F/v_m^p}{F/v_m^p + (1 - F)/v_m^m}, \tag{52}$$

where v_m^m is the molar volume of the matrix phase.

In its turn, the volume fraction of precipitates may be calculated from the distribution function

$$F = \frac{4\pi}{3}\int\limits_0^\infty f(R, t)R^3 dR \tag{53}$$

These equations determine the evolution of precipitate ensemble at the stage of coarsening. Lifshitz and Slezov [53] solved this problem in the asymptotic limit.

Particularly, they demonstrated that in the limit $t \to \infty$ the critical radius temporal dependence is characterized by the power law:[1]

$$R_c^3 - R_{c0}^3 = Kt, \tag{54}$$

where R_{c0} is the critical radius which the system has at an initial moment of the stage, when the process can be described by asymptotic equations, and K is a constant equal to [54]:

$$K = \frac{4Dl^m}{9(C^p - {}^eC^m)}. \tag{55}$$

Besides, they demonstrated that there exists a universal distribution function, which does not depend on time and describes PSD in an asymptotic limit. This function is of the following form:

$$P(u) = \begin{cases} \frac{3^4 e}{2^{5/3}} \cdot \frac{u^2 \exp\{-1/[1-(2/3)u]\}}{(u+3)^{7/3}[(3/2)-u]^{11/3}}, & u < 3/2 \\ 0 & u > 3/2 \end{cases} \tag{56}$$

where $u = R/R_c$ is the relative radius of precipitates; $P(u)$ is the probability density function ($P(u)du$ is the probability that a particle has a radius in the range between R and $R + dR$).

Later on the solutions of the problem of coarsening at the asymptotic stage controlled by other mechanisms of mass transfer were obtained in [55–57]. The solutions for various mechanisms of mass transfer are reviewed in [58, 59], and some specifications of these solutions are given in [60]. All these solutions were also obtained for infinitesimal volume fraction of the second phase. Solutions for coarsening in multicomponent systems were obtained in [61–65].

In a number of studies the coarsening of carbide and nitride precipitates in steels was investigated [66–69]. Particularly, it was shown that carbide and nitride coarsening in the temperature range of austenite, as a rule, is controlled by volume diffusion, whereas at lower temperatures, in ferrite, the process may be controlled by other mechanisms of mass transfer.

Specific features of theoretical description of carbide and nitride coarsening are associated with the necessity to consider multicomponent diffusion, including the simultaneous diffusion of interstitial and substitutional elements. The coarsening of stoichiometric $(Fe,M)_a C_b$ carbides in austenite is considered in [69], where the following expression was obtained to describe their radius variation:

$$\overline{R}^3 - \overline{R}^3 = \frac{8(a+b)\sigma v_m^p D_M^{\gamma}\, {}^eC_M^{\gamma}}{9aR_g T(C_M^p - {}^eC_M^{\gamma})^2}t \tag{57}$$

It was shown in [69], that at the stage of coarsening this equation satisfactorily describes the carbide precipitate evolution in austenite.

---

[1] In Lifshitz-Slezov's theory at an asymptotic stage the critical radius is equal to the average one.

The limitation of the infinitesimal volume fraction of precipitating phase used in the Lifshitz-Slezov's theory was one of its main drawbacks, because the available experimental results show that the volume fraction of precipitates affect the rate of the average particle size increasing and the form of the distribution function. Quite a few theories were suggested to overcome this drawback. One of the ways to solve the problem for a non-zero volume fraction of precipitates is using the mean field or effective environment approximations. In this case the rate of particle growth for every particle size range is formulated through interaction between a particle and its average surrounding. The main feature of such theories is the statistic field cell connected with every particle. Every cell is a spherical domain concentrically enveloping a particle, and contains a particle and matrix volume connected with it with a local averaged diffusion field. In this case the diffusion interaction in field cells connected with particles is considered. Mass exchange between particles is realized through cell walls, the concentration on the boundaries of which is equal to the average concentration in the matrix, i.e. the boundary condition (46) is substituted for

$$C^m\left(r = R^L\right) = \overline{C}^m. \tag{58}$$

This model is shown schematically in Fig. 14.

Some coarsening models based on the mean field approximation are reviewed in [70, 71].

The mean field approximation requires some assumptions relating the average extension of transport field connected with a particle (that is, its sphere of influence) with the particle size and the volume fraction of precipitating phase.

Various modes of construction of field cells were suggested in [70, 72, 73], from purely geometrical to those based on more complicated criteria. Thus, for example, in [73] the cell sizes were calculated from the self-similarity criterion. The growth constant in Eq. (55) and the form of distribution function depend on the choice of field cells.

Fig. 14 Geometrical sketch of coarsening models constructed based on the mean field approximation
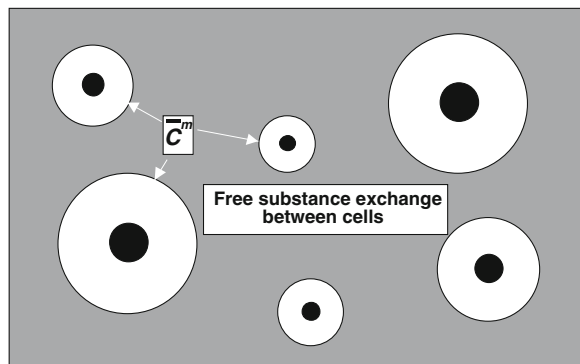
Along with the above cited publications [70–73], there are several more studies in which the theories were worked out, taking into account the influence of the second phase finite volume fraction, particularly, [74–77].

The numerical simulation of precipitates behavior at coarsening has grown in popularity recently [78–82]. In case of numerical simulation one can analyze the precipitate behavior not only at the asymptotic stage, but also at the non-stationary stage, when the equilibrium phase composition has been almost reached and the PSD is far from the asymptotic one yet. Besides, in numerical simulation the systems with high volume fraction of precipitates may be analyzed, when because of the particles proximity to each other the diffusion fields near their surfaces get considerably non-uniform and the particle shape deviate from the spherical one.

Elastic stresses arising from the particle growth may have a profound effect on coarsening. There are many examples of such effect, which are reviewed in [71]. For instance, in systems in which the stresses originate from the misfit of particle–matrix crystal lattices, an almost random spatial distribution of particles, resulting from nucleation and growth, may evolve into highly correlated spatial distribution, in which particles are arranged into rows along elastically soft crystallographic directions in the matrix, or into almost periodical ensembles. Besides, the elastic stresses strongly affect the morphology of some particles. At coarsening the initially spherical particles can change their shape and divide into smaller particles. Recently great attention has been paid to the numerical simulation of precipitates coarsening, taking into account the arising elastic stresses, as it is very difficult to describe this process analytically because of great complexity of the accompanying phenomena, and considerable success was achieved in this direction [83–85].

4 Simulation of Different Stages of Precipitate Evolution

It is not possible to solve by analytical methods a multi-particle diffusion problem in such general form, that the solution would describe precipitate evolution at all stages of the process, even for binary systems.

The methods of numerical simulation of precipitates evolution until recently were also worked out mainly for this or that concrete stage of the process. The methods of simulation of growth and dissolution considered in Sect. 2, do not provide taking into account the polydispersity of precipitates ensemble, and, consequently, they cannot be generalized for the stage of coarsening and for transition stages from growth or dissolution to coarsening, when the polydispersity of the ensemble and the form of PSD determine the system behavior. The available methods of simulation of precipitates evolution at the coarsening stage also have a number of limitations [78–82]. Firstly, they deal, as a rule, with binary systems, and secondly they suggest that the volume fraction of precipitates is close to equilibrium, which makes it impossible to use them for the stages of growth or dissolution.

In our recent studies [86–92] a method was worked out for simulation of precipitates evolution in binary and multi-component systems at different stages in the framework of one and the same model, taking into account the precipitates ensemble polydispersity. This section is to describe this method and analyze its capabilities. At first we consider simulation of precipitates ensemble in two-phase binary alloys, then possibilities of its generalization to the case of multiphase systems are analyzed, and, finally, the evolution of precipitates ensemble is considered taking into account the formation of new nuclei.

The method is based on the mean field model, and several assumptions were used for its development. It is assumed that the particles have spherical shape and constant composition, equilibrium concentrations of components are established at interfaces and the process is controlled by volume diffusion.

4.1 Binary Systems

The main problem to be solved in simulation of precipitates evolution in alloys is to find velocities of interfaces. An interface velocity for a particle of radius R can be determined from the mass balance equation, which for a binary system has the form (2).

To find an interface velocity one must know the solute concentration gradient in the matrix at an interface with the particle, i.e., it is required to know the solute concentration distribution in the particle surrounding. Thus, one must solve the diffusion Eq. (1) at the appropriate initial and boundary conditions.

Various models of the processes of growth, dissolution and coarsening differ, first of all, by the mode of assignment of boundary conditions used to find solute concentration distribution in a particle surrounding.

We used the mean field approximation, i.e., we considered diffusion interaction of particles with the matrix in field cells. In this case one must know boundary conditions for an interphase boundary and cell boundary.

In case of a binary system, when the process is controlled by diffusion, it is not difficult to give the condition for precipitate/matrix interface, as it is an assignment of boundary concentration which is determined by the local equilibrium conditions at an interface.

It is more difficult to determine conditions at cell boundaries. As was demonstrated before, in simulation of dissolution and growth processes it is assumed that the dissolved component concentration gradient at a cell boundary is equal to zero, whereas in the description of coarsening it is supposed that the concentration at a cell boundary is equal to the average concentration in the matrix.

To consider diffusion growth, dissolution and coarsening of precipitates in the framework of one model, one must find such boundary conditions which would be suitable for simulation of all three processes, and it was done in [86]. It was assumed that at cell boundaries of all size intervals one and the same solute component concentration, C^L, is established, but its value is not known a priori.
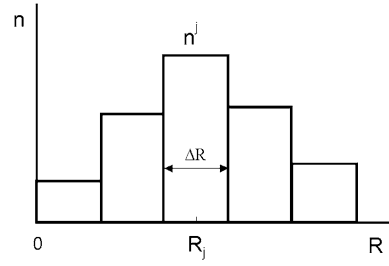
The initial data for simulation of precipitate ensemble evolution were the precipitate volume fraction and PSD in the initial state. The PSD was given by a histogram, i.e., a fraction of particles n^j, falling in the j-th interval of particle radii from $R_j - \Delta R/2$ to $R_j + \Delta R/2$, is associated with this size interval. Here R_j is the average radius of particles of the j-th size, and ΔR is the width of this interval (for all size intervals this value was taken the same). The scheme of PSD is shown in Fig. 15.

We used three modes of construction of field cells, illustrated by Fig. 16, which are in many respects analogous to the models worked out for the description of coarsening in systems with finite volume fraction of precipitates.

Model I (Fig. 16a). The cell radius is proportional to the particle radius and calculated by the formula:

$$R_j^L = R_j \cdot F^{-1/3}, \tag{59}$$

were R_j^L is the influence sphere radius corresponding to the j-th size interval. This model is completely analogous to that suggested in [70].

Model II (Fig. 16b). Cell radii are the same independently on the particle sizes. This model was suggested in [93], but we used another way of calculating cell sizes. The cell radius was calculated by the formula:

$$R^L = \left(\sum_{j=1}^{N_p} n^j R_j^3 / F \right)^{1/3}, \tag{60}$$

where N_p is the number of size intervals.

Model III (Fig. 16c). The cell radius is combined from the particle radius and a half of mean distance between particle surfaces $\overline{L}$:

$$R_j^L = R_j + \frac{\overline{L}}{2} \tag{61}$$

For this model there are various ways of estimation of the mean distance between particle surfaces. We estimated it using the following expression, linking the mean distance between particles, PSD and precipitates volume fraction:
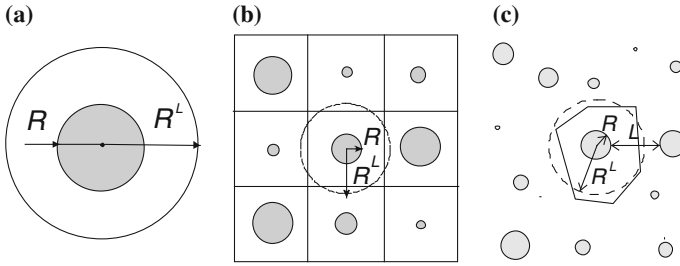
Fig. 16 Geometrical models of field cells: **a**–model I, **b**–model II, **c**–model III

$$F = \frac{\sum\limits_{j=1}^{N_p} n^j R_j^3}{\sum\limits_{j=1}^{N_p} n^j \left(R_j + \frac{L}{2}\right)^3} \qquad (62)$$

To find component concentration distributions in cells, the stationary diffusion Eq. (44) was used. The feasibility of stationary approximation for coarsening is beyond question. The possibility to use it for growth and dissolution is less obvious. As mentioned above, the solution obtained using the stationary field approximation is the more exact, the less is the value of the $\lambda = \frac{C^{m/p} - {}^0 C^m}{C^p - C^{m/p}}$ parameter. That is why for small enough λ ($< \sim 0.1$) the use of the stationary approximation is quite correct not only for coarsening, but for other stages as well.

Using the stationary approximation, the following expressions are obtained for concentration distributions of the solute component in cells:

$$^j C^m(r) = \frac{{}^j C^{m/p} - C^L}{\left(1/R - 1/R_j^L\right)} \frac{1}{r} + \frac{C^L R_j^L - {}^j C^{m/p} R}{R_j^L - R}, \qquad (63)$$

where $^j C^m(r)$ is the solute component concentration in a cell of the j-th size interval; $^j C^{m/p}$ is the solute component concentration at interfaces with particles of the j-th size interval; and C^L is the solute component concentration at a cell boundary (for the cells of all size intervals it is taken the same).

Concentration at a particle/matrix interface was given by the Gibbs–Thomson equation, according to which for every size interval:

$$^j C^{m/p} = {}^e C^m \exp\left(\frac{2\sigma v_m^p}{R_g T} \frac{1 - {}^e C^m}{C^p - {}^e C^m} \frac{1}{R_j}\right). \qquad (64)$$

The calculated concentrations of components in matrix must satisfy the mass conservation condition (50).

The solute component average concentration in the matrix is connected with concentration distributions in cells and the mole fraction of precipitates with its volume fraction by the following relationships:

$$\overline{C}^m = \frac{3 \sum\limits_{j=1}^{N_p} n^j \int\limits_{R_i}^{R_i^L} {}^j C r^2 dr}{\sum\limits_{j=1}^{N_p} n^j \left[(R_j^L)^3 - (R_j)^3 \right]}, \tag{65}$$

and

$$\alpha_p = \frac{F/V_m^p}{F/V_m^p + (1-F)/V_m^m}. \tag{66}$$

In the case considered the mass conservation condition must be added explicitly, as in the diffusion equation the time derivative is neglected. The mass conservation condition takes into account that if the average concentration of the solute component in the matrix depends on time, then the volume fraction of precipitates is time dependent as well.

Substitution of (63) in Eq. (2) gives expressions for interface velocities:

$$V_j = \frac{dR_j}{dt} = \frac{D}{\left(C^p v_a^m / v_a^p - {}^j C^{m/p} \right)} \frac{\left(C^L - {}^j C^{m/p} \right)}{\left(R_j^L - R_j \right)} \frac{R_j^L}{R_j} \tag{67}$$

A step-by-step procedure was used in calculations, and based on the volume fraction and PSD at time t these parameters were calculated for the moment $t + \Delta t$. The calculation procedure was as follows.

1. Based on values of volume fraction F, the average concentration of the solute component in the matrix, $\overline{C}^m$, was calculated using expressions (50) and (66).
2. Cell sizes were calculated using expressions (59, 60) or (61).
3. Concentration at cell boundaries, C^L, was calculated as follows. After the substitution into (65) of expressions of concentration distributions in cells (63) and expressions of the solute component boundary concentrations (64), one obtains an equation with one unknown, C^L, which is calculated numerically and gives concentrations at cell boundaries.
4. The interface velocities were calculated by Eq. (67).
5. The particle radii R'_j and their volume fraction F' at a new time step were found from:

$$R'_j = R_j + V_j Dt \tag{68}$$

and

Fig. 17 The scheme of
calculation of PSD at a new
time step
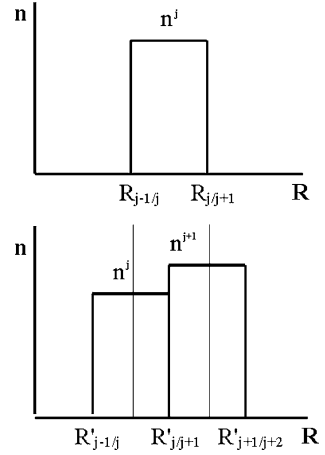
$$F' = \frac{\sum\limits_{j=1}^{N} n^j R_j'^3}{\sum\limits_{j=1}^{N} n^j R_j^{L^3}}. \tag{69}$$

6. The PSD at a new time step was calculated, a special procedure being used for that.[2] Let's illustrate this procedure by an example of determining the fraction of particles in the j-th size interval at a new time step. The boundaries of the j-th interval are denoted as $R_{j-1/j}$ and $R_{j/j+1}$ ($R_{j-1/j} = R_j - \Delta R/2$, $R_{j/j+1} = R_j + \Delta R/2$). For the time Δt the particle radii change, and the new radii, corresponding to the boundaries of the division intervals $R'_{j-1/j}$ and $R'_{j/j+1}$ can be calculated from the formulas similar to (64, 68) and (69). After that in the initial size interval from $R_{j-1/j}$ to $R_{j/j+1}$ there may be no particles, which were in that interval at the previous time step, or only a part of them may remain. At the same time at the new time step in this size interval may fall the particles which belonged to other size intervals at the previous time step. Let, for example, in the size interval from $R_{j-1/j}$ to $R_{j/j+1}$ at a new time step the particles, which belonged to the j-th and $(j+1)$-th intervals fall partly, as it is shown in Fig. 17.

---

[2] To find the PSD at a new time step it would be natural to use the continuity equation in the size space (49). However it appeared inconvenient in numerical calculations, when the distribution function is given not analytically, but by a histogram. Particularly, a fraction of particles in some size intervals, calculated by the continuity equation in difference form, may appear to be negative.

Then the fraction of particles of the j-th interval at a new time step can be calculated by the formula:

$$n'^j = \frac{R'_{j/j+1} - R_{j-1/j}}{R'_{j/j+1} - R'_{j-1/j}} n^j + \frac{R_{j/j+1} - R'_{j/j+1}}{R'_{j+1/j+2} - R'_{j/j+1}} n^{j+1}. \tag{70}$$

Taking into account that a part of particles dissolve at a new time step (there radii get smaller than that corresponding to the lower boundary of the first size interval), the values obtained from the formulas like (71) must be normalized.

The as-determined values of volume fraction and PSD served as the initial ones for calculations at a new time step. This procedure was repeated till the required time was achieved.

This technique of calculation was tested in [86–88], and the comparison of calculation results with the available experimental data demonstrated their good agreement. It was also shown that calculations made with various geometrical models of field cells give closely similar results in case of a relatively low volume fraction of precipitates (not more than several percents). That is why only Model I was used in simulation of carbide and nitride precipitates evolution.

4.2 Multicomponent Alloys

The method described in the previous section was generalized to the case of multicomponent low-alloyed alloys in [89–91], the same assumptions as for binary alloys being used. The problem for multicomponent alloys is more complicated, as component concentrations at interfaces in this case are unknown. In case of low-alloyed alloys the matrix may be considered as a dilute solution, which allows not taking into account concentration dependences of diffusion coefficients and interaction of components in the solution, i.e., impurity diffusion may be considered instead of interdiffusion. In this case the concentration distributions of components in cells are expressed analytically with the relationships similar to (64):

$$^jC_i^m(r) = \frac{^jC_i^{m/p} - C_i^L}{\left(1/R_j - 1/R_j^L\right)} \frac{1}{r} + \frac{C_i^L \cdot R_j^L - {}^j C_i^{m/p} \cdot R_j}{R_j^L - R_j}, \tag{71}$$

where $^jC_i^m(r)$ is the concentration of the i-th component in the matrix in a cell of the j-th size interval; $^jC_i^{m/p}$ is the concentration of the i-th component in the matrix at an interface with particles of the j-th size interval; and C_i^L is the concentration of the i-th component at cell boundaries.

The mass balance conditions at interphase boundaries are:

$$\left[C_i^p V_m^m / V_m^p - {}^jC_i^{m/p}\right] \frac{dR_j}{d\tau} = D_i \frac{d^jC_i^m}{dr}\bigg|_{r=R_j}, \tag{72}$$

where D_i is the impurity diffusion coefficient of the i-th component in the matrix.

After substitution of expressions (71) for component concentration distributions in cells into Eq. (72), the latter take the form:

$$\left[C_i^p V_m^\alpha / V_m^p - {}^jC_i^{m/p}\right] \frac{dR_j}{d\tau} = D_i \frac{{}^LC_i - {}^jC_i^{m/p}}{R_j^L - R_j} \cdot \frac{R_j^L}{R_j} \tag{73}$$

For the case of precipitates of constant composition $A_aB_b\ldots$, the equilibrium condition at a particle/matrix interface with the correction for the interface curvature is:

$$a^j\overline{G}_A^{m/p} + b^j\overline{G}_B^{m/p} + \cdots - \frac{2\sigma V_m^p}{R_j} = {}^0G_{A_aB_b\ldots}, \tag{74}$$

where ${}^jC_i^{m/p}$ is the chemical potential of the i-th component in the matrix at an interface with a particle from the j-th size interval.

In case of sparingly soluble compounds the local thermodynamic equilibrium condition at an interface can be determined as:

$$L_{A_aB_b\ldots}(R_j) = L_{A_aB_b\ldots} \exp\left(\frac{2\sigma V_m^p}{R_g T} \frac{1}{R_j}\right), \tag{75}$$

where $L_{A_aB_b\ldots}(R_j)$ and $L_{A_aB_b\ldots}$ are the solubility product for the particles of the j-th size interval and the equilibrium value of the solubility product, respectively.

The mass conservation condition in this case is

$$\alpha_p C_i^p + \left(1 - \alpha_p\right)\overline{C}_i^m = C_i^{al}. \tag{76}$$

The mole fraction is connected with the volume fraction of precipitating phase by relationship (66).

The step-by-step procedure was used in calculations, as it was done for binary alloys, and based on the volume fraction and PSD for time t these parameters were determined for $t + \Delta t$. The calculation procedure was to a great extent similar to that for calculations of precipitates evolution in binary alloys. The calculation order was as follows.

1. Calculation of average concentrations of components in the matrix based on the value of the precipitating phase volume fraction Eqs. (66, 76).
2. Calculation of field cells sizes [expressions (59, 60 or 61)].
3. Calculation of interface velocities for particles from different size intervals.

The calculation of interface velocities in case of multicomponent alloys is much more difficult than in case of binary systems. Particularly, it is so because for

multicomponent systems the component concentrations at interphase boundaries
are not known a priori.

Calculations of concentration distribution in cells and interface velocities were
performed based on the requirement that the values of average concentrations of
components in the matrix must satisfy the mass conservation condition. This
means that the average component concentrations in the matrix calculated from the
volume fraction of precipitating phase must be equal to average concentrations,
calculated based on the component concentration distribution in field cells. Thus,
for the $(N + 1)$-component system the component concentration distributions in
field cell must satisfy the system of N equations:

$$\Phi_i = \overline{C}_i^m - \frac{3 \sum\limits_{j=1}^{N_p} n^j \int\limits_{Rj}^{R_j^L} {}^jC_i^m r^2 dr}{\sum\limits_{j=1}^{N_p} n^j \left[(R_j^L)^3 - (R_j)^3 \right]} = 0 \qquad (77)$$

In these equations the first member in the right part corresponds to the average
concentration calculated from the volume fraction, and the second one to the
average concentration determined from concentration distributions in cells.

From expressions (71) for component concentration distributions in cells one
can see that they are determined by concentrations at interphase boundaries and
cell boundaries. In their turn, the component concentrations at interphase bound-
aries and the velocities of the latter for every size interval can be calculated from
concentrations at cell boundaries by the combined solution of mass balance Eq.
(73) and thermodynamic Eqs. (74) or (75). Thus, having specified the concen-
trations at cell boundaries, one can calculate interface velocities, determine
component concentration distributions in cells and calculate the values of Φ_i
function. This was the algorithm of solution of system (77), which resulted in
determination of interface velocities.

The calculation order was as follows:

a. Initial approximations of concentrations at cell boundaries were given.
b. Interface velocities and boundary concentrations were calculated from com-
   bined solution of mass balance Eq. (73) and thermodynamic Eqs. (74) or (75).
c. The values of functions Φ_i were calculated in a point corresponding to the initial
   approximations and in its vicinity.
d. The derivatives of Φ_i functions with respect to C_i^L were found by numerical
   differentiation in the point corresponding to the initial approximations.
e. The corrected values of concentrations at field cell boundaries were calculated
   by the Newton-Raffson method based of the determined values of the functions
   and their derivatives.
f. The values of C_i^L obtained from the cycle (b–e) were used as the initial approx-
   imations for a new iteration, i.e., the calculation was repeated from point (b).
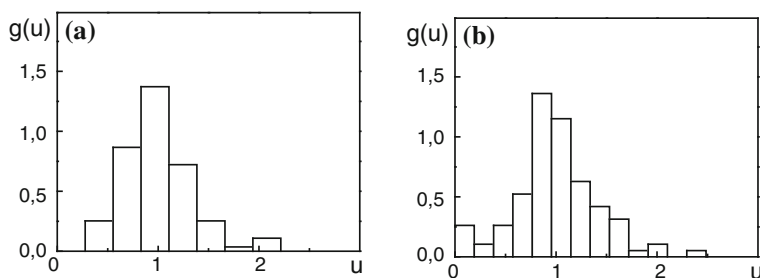
Fig. 18 Initial PSDs of AlN [94]: **a**–annealing at 650 °C, 24 h; **b**–annealing at 700 °C, 24 h

The iteration cycle was over if the following iteration differed from the previous one by the value less than the given convergence accuracy. The values of interface velocities and concentrations at interfaces and field cell boundaries were found by this iteration procedure.

4. Calculation of particles radii and their volume fraction at a new time step by formulas (5.68–5.69).
5. Calculation of PSD at a new time step by the procedure described above for binary systems based on the analysis of the number of particles leaving the initial size interval and falling in it from other intervals due to the growth or dissolution [see Fig. 17 and expression (70)].

The as-determined values of volume fraction and PSD served as the initial ones for calculations at a new time step.

In [90–92] the calculation results for evolution of AlN and MnS precipitates in austenite and ferrite are compared to the available experimental data at different stages of evolution, and their good agreement is demonstrated.

Let's illustrate this by an example of the comparison of calculation results with the experimental studies on AlN evolution in austenite at the stage of dissolution and the following coarsening carried out in [94].

The steel under study contained 0.038 wt. % C, 0.30 wt. % Mn, 0.040 wt. % Al and 0.007 wt. % N. Different initial PSDs of AlN were obtained by preliminary heat treatments. The first initial distribution was obtained by 650 °C annealing, and the second one by 700 °C for 24 h. The PSDs resulting from these treatments are shown in Fig. 18. It is obvious that they differ considerably, as the annealing at 650 °C ensures more dispersed precipitates than that at 700 °C. In both cases practically complete bonding of N in nitrides was achieved. The as-obtained PSDs and the volume fraction corresponding to complete bonding of N in nitrides (0.00048) served as the initial data for simulation.

Figure 19 demonstrates calculated temporal dependences of volume fractions of precipitates for two temperatures, 1,000 and 1,100 °C. It is seen that at short times of heat treatment the volume fraction drastically reduces, which results from dissolution of the exceeding phase. The intensive dissolution occurs during a very

Fig. 19 Calculated
dependences of AlN volume
fraction on the annealing time
for 1,000 and 1,100 °C.
Initial state–annealing at
700 °C, 24 h
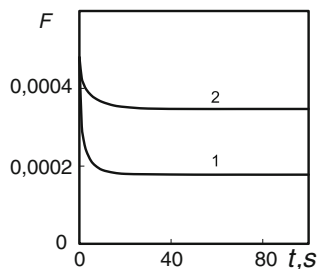
short period of time, several tenths of seconds. This time appears to be enough for
an achievement of phase composition close to equilibrium. At further holding the
volume fraction stabilizes and does not change with growing annealing time. The
stage of dissolution is finished and coarsening starts, the volume fraction
remaining almost unchanged.

Figure 20 demonstrates comparison of calculated and experimental depen-
dences of precipitates average radius on the annealing time. These dependences
are shown for different initial PSDs and for two annealing temperatures, 1,000 and
1,100 °C. It is seen that in all the cases calculations describe the evolution of
precipitates average size quite well.

The difference between simulation results and experimental data, as a rule, does
not exceed experimental error. As seen from these dependences, at first the average
radius of precipitates somewhat decreases. It may be explained by the precipitates
dissolution, all the particles dissolving at the beginning. It is interesting to note that
the average particle sizes due to the dissolution change only slightly. It means that
though the sizes of all particles are decreasing, fine particles dissolve faster, and
their fraction reduces. As a result, the average size of precipitates does not change
considerably even in case of relatively high extent of the second phase dissolution.
The stage of dissolution proper, at which the second phase volume fraction is
reduced, is quickly finished, and the coarsening starts, at which coarser particles
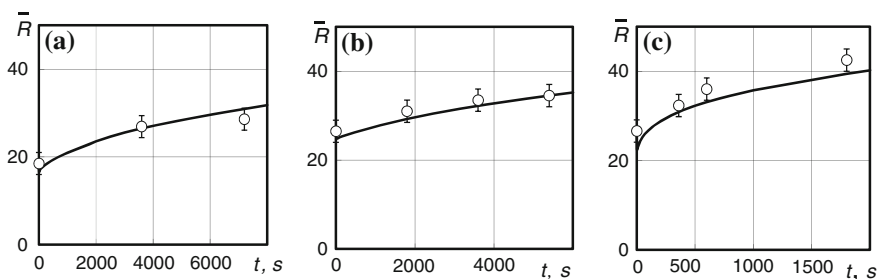

Fig. 20 Comparison of calculated and experimental [94] dependences of AlN precipitates
average radius on the annealing time for 1,000 (**a, b**) and 1,100 °C (**c**): a–initial state is after
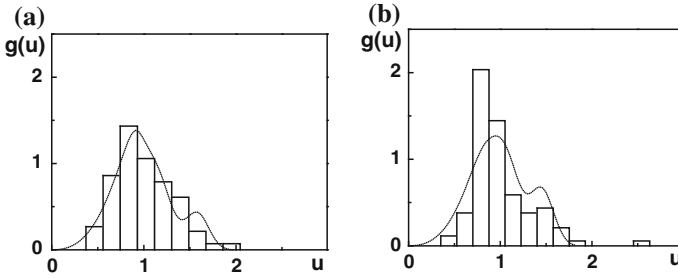650 °C, 24 h annealing

Fig. 21 Comparison of calculated (*lines*) and experimental (histograms) [94] AlN PSDs after the annealing at 1,000 °C for 1 (**a**) and 2 h (**b**). Initial state–annealing at 650 °C, 24 h (u = R/$\overline{R}$)
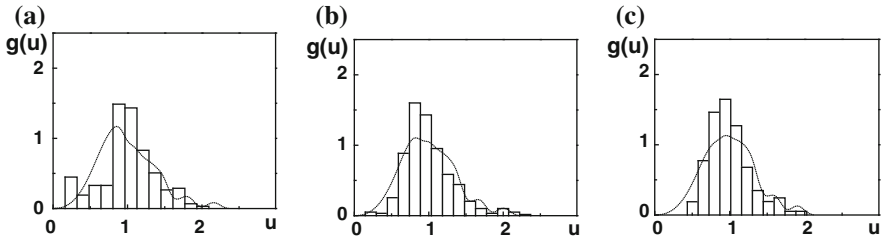

Fig. 22 Comparison of calculated (*lines*) and experimental (histograms) [94] AlN PSDs after annealing at 1,000 °C for 0.5 (**a**), 1 (**b**) and 2 h (**c**). Initial state–annealing at 700 °C, 24 h (u = R/$\overline{R}$)

grow fast and the finer ones dissolve. At this stage the average particle size is increasing, whereas their volume fraction almost does not change.

Figures 21 and 22 demonstrate comparison of calculated and experimental PSDs of AlN after the different time annealing at 1,000 °C for two initial states. It is seen that these distributions are in quite a good agreement, which allows concluding that the numerical method suggested in the present work describes adequately the PSD evolution at annealing. Some difference in calculated and experimental distributions is obviously due to experimental errors, particularly, the errors in the initial distributions which serve as the initial data for simulation.

These examples show that the calculated dependences of precipitates average radius and PSDs are in very good agreement with the experiment. In [89–91] calculated and experimental dependences of average particles radius, their volume fraction and PSDs for different stages of precipitates evolution in austenite and ferrite of low-alloyed steels are compared, and quite a good agreement is found as well.

In the general case of medium- and high-alloyed alloys the calculation is more complicated, as one must consider interdiffusion, but not the impurity diffusion,

and take into account components interaction in solid solution and concentration dependences of interdiffusion coefficients. This case is considered in [92].

In the case considered the system of stationary diffusion equations describing diffusion in a cell of the j-th size interval for the $(N + 1)$-component alloy takes the form:

$$\frac{\partial}{\partial r}\left(r^2 \sum_{l=1}^{N} \widetilde{D}_{il} \frac{\partial^j C_l}{\partial r}\right) = 0. \tag{78}$$

The following equations describing component concentration distributions in cells are obtained from these equations:

$$\sum_{j=1}^{N} \widetilde{D}_{ij} \frac{\partial^l C_j}{\partial r} = \frac{K_i^l}{r^2}, \tag{79}$$

where K_i^l is a constant for every element and every size interval.

Component concentrations at interphase boundaries must satisfy the local equilibrium and mass balance conditions. For precipitates of constant composition, $A_a B_b \ldots$, equilibrium conditions at particle/matrix interfaces are expressed by Eq. (74). Concentrations at cell boundaries must be equal.

The mass balance condition is:

$$\left[C_i^p v_a^m / v_a^p - {}^l C_i^{m/p}\right] \frac{dR_l}{d\tau} = \sum_{j=1}^{N} \widetilde{D}_{ij} \frac{\partial^l C_j^m}{\partial r}\bigg|_{r=R_l}, \tag{80}$$

or, taking into account (79), it is:

$$\left[C_i^p v_a^m / v_a^p - {}^l C_i^{m/p}\right] \frac{dR_l}{d\tau} = \frac{K_i^l}{(R_l)^2}. \tag{81}$$

The calculation procedure is in general analogous to that described above for low-alloyed alloys, but in this case the calculations are much more complicated, as the component concentrations in cells cannot be given analytically, and numerical methods must be used to find them. We used the finite difference method. For field cells of all size intervals spatial nets were constructed, the first node of which (node 0) coincided with an interphase boundary, and the last one (node n) with a cell boundary. Concentrations in cells were given as net functions determined in discrete nodes of the net, ${}^j C_i(k)$, where j is the number of the size interval, and k is the number of the spatial net node. Thus, the i-th element concentration at an interface with a particle of the j-th size interval is denoted as ${}^j C_i(0)$, and its concentration at a cell boundary as ${}^j C_i(n)$.

The spatial net construction in a field cell of the j-th size interval is shown in Fig. 23. The k-th node coordinates in the j-th size interval cell are denoted as ${}^j r(k)$.

Fig. 23 The sketch of spatial net construction in the j-th size interval cell and concentration distribution of the i-th element in it
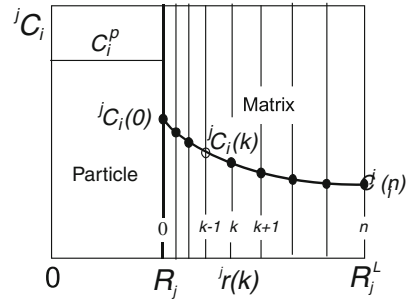
The calculation order is as follows.

1. Calculation of average component concentrations in the matrix by Eqs. (66) and (76) based on the precipitate volume fraction.
2. Calculation of field cell sizes. Dependently on the geometrical model used, the field cell radii were calculated by expressions (59, 60 or 61).
3. Construction of spatial nets in field cells of different size intervals, making allowance for non-uniform spatial nets refined maximally near interpose boundaries.
4. Calculation of concentration distributions and interface velocities for particles from different size intervals.
5. Calculation of particles radii and their volume fraction at a new time step from formulas (68–69).
6. Calculation of PSD at a new time step using the above-described for binary systems procedure, based on the analysis of the number of particles leaving the initial size interval and falling in it from other intervals due to growth or dissolution.

The as-determined values of volume fraction and PSD served as the initial ones for calculations at a new time step.

The most difficult part of calculations is the calculation of concentration distributions in cells and interface velocities. It is carried out based on the requirement that average component concentrations in the matrix, calculated from the precipitate volume fraction, are equal to the average concentrations, calculated from concentration distributions of components in field cells, i.e., component concentrations in cells must satisfy the system of N equations of the form:

$$\Phi_i = \overline{C}_i^m - 3 \left\{ \sum_{j=1}^{N_p} n^j \sum_{k=0}^{n-1} \frac{\left[{}^jC_i(k+1)({}^jr(k+1))^2 + {}^jC_i(k)({}^jr(k))^2 \right]}{2} \left[{}^jr(k+1) - {}^jr(k) \right] \right\} / $$

$$\left\{ \sum_{l=1}^{N} n^l \left[(R_l^L)^3 - (R_l)^3 \right] \right\} = 0$$

$$(82)$$

The first member in the right part of Eq. (82) corresponds to the average component concentration in the matrix calculated from the precipitate volume fraction, and the second one corresponds to the average concentration calculated from component concentrations in spatial net nodes for field cells of all size intervals.

The calculation was as follows:

1. Initial approximations for component concentrations at cell boundaries were given.
2. Based on the component concentrations at cell boundaries for each size interval component concentration distributions and interface velocities were calculated.
3. The values of function Φ_i were calculated in the points corresponding to the initial approximations and their vicinity.
4. The values of function Φ_i derivatives with respect to C_i^L in the point corresponding to the initial approximations were found by numerical differentiation.
5. Based on the as-found functions and their derivatives the refined values of concentrations at field cell boundaries were calculated by Newton–Raphson method.
6. The values of C_i^L obtained from the cycle (points 2–5) were used as the initial approximations for a new iteration, i.e., the calculation was repeated from point 2.

The iteration cycle was over if the following iteration differed from the previous one by a value less than the given convergence accuracy. The interface velocities and concentrations at interphase and field cell boundaries were found from this iteration procedure.

Component concentrations in cells and interface velocities are calculated based on the requirement that component concentration at particle/matrix interfaces and interface velocities satisfy the local equilibrium and mass balance conditions. These equations in case of net variables take the form:

$$FT^j = a\overline{G}_A^{\alpha/p}\left[{}^jC_1(0),\ldots,{}^jC_N(0)\right] + b\overline{G}_B^{\alpha/p}\left[{}^jC_1(0),\ldots,{}^jC_N(0)\right] + \ldots - \frac{2\sigma v_m^p}{R_j} - {}^0G_{A_aB_b\ldots} = 0 \quad (83)$$

$$FB_i^j = \left[C_i^p\bar{v}_a^m/\bar{v}_a^p - {}^jC_i(0)\right]\cdot V_j - \frac{K_i^j}{R_j} \quad (84)$$

To calculate concentration distributions in cells Eq. (80) was used, the difference approximation of which is:

$$\sum_{l=1}^{N}\widetilde{D}_{il}\frac{{}^jC_l(k+1) - {}^jC_l(k)}{{}^jr(k+1) - {}^jr(k)} = \frac{4K_i^j}{\left[{}^jr(k+1) + {}^jr(k)\right]^2} \quad (85)$$

For field cells of each size interval concentration distributions and interface velocities were calculated separately. The calculation order was as follows:

a. Initial approximations for constants K_i^j and interface velocity V_j were given.

b. Component concentration distributions in a field cell were calculated by Eq. (85).
c. The values of functions FT^j and FB_i^j were calculated in the points corresponding to the initial approximations and their vicinity.
d. The values of FT^j and FB_i^j derivatives with respect to K_i^j and V_j in a point corresponding to the initial approximations were found by numerical differentiation.
e. Based on the as-determined values of the functions and their derivatives the refined values of constants K_i^j and interface velocities V_j were calculated by the Newton-Raffson method.

The values of K_i^j obtained from the cycle (b–e) were used as initial approximations for a new iteration, and the calculation was repeated from point b.

The algorithm generalized on the case, when the matrix was not a dilute solution and one must take into account components interaction in solid solution and concentration dependences of interdiffusion coefficients, was tested in [92]. The calculation results were compared to the experimental data on the behavior of VC precipitates in austenite of steel with 1.1 wt. % V and 0.86 wt. % C from [69]. The heat treatment was as follows. Specimens were quenched in water from 1,300 °C and then heated to 700 °C and held for 5 h to obtain dispersed spherical precipitates, and, finally, they were annealed at 900–1,100 °C for 10–200 h. At such preliminary treatment the alloy before annealing consists of austenite matrix with very fine precipitates of vanadium carbide. The precipitates volume fraction is considerably less than equilibrium, i.e., the solid solution is highly supersaturated.

Comparison of the calculation results with the experimental data demonstrates that for the 1,100 °C annealing they are in quite a satisfactory agreement both for the average particle sizes and PSDs. However, for lower annealing temperatures calculation results markedly differ from the experimental data. In [92] it is suggested that this difference is mainly because the possibility of new nucleation centers was not taken into account in calculations. At 1,100 °C the supersaturation of solid solution is not very high, and the formation of new nuclei is hardly probable, but at lower annealing temperatures it is quite possible. That is why in calculations the formation of new nucleation centers must be taken into account.

4.3 Simulation of Precipitates Evolution with Consideration for Nucleation

As shown in the previous section, simulation of precipitates evolution without considering nucleation in some cases results in considerable discrepancy in calculations and experiment.

The calculation algorithm taking nucleation into account was suggested in [99]. According to this publication, we consider simulation of precipitates evolution with consideration for nucleation by an example of vanadium carbides.

The nucleation rate was calculated based on the classical theory of nucleation. We used an approach developed by Liu and Jonas [95, 96], who showed that if the nuclei are formed on dislocations, then the nucleation rate and the Gibbs energy of a critical sized nucleus may be calculated from the formulas:

$$\mathrm{J} = \rho\, D_{eff}\, C/a^3 \exp\left(-\frac{\Delta G_{crit}}{k_B T}\right),$$

(86)

and

$$\Delta G_{crit} = \frac{16\pi\zeta^3 \sigma_n^3}{3(\Delta G_{chem} + \Delta G_{\varepsilon})}.$$

(87)

Here ρ is the dislocation density, a is the lattice parameter of a matrix, k_B is the Boltzmann constant, D_{eff} and C are the effective diffusivity and concentration of the element controlling the rate of nucleation, σ_n is the specific surface energy of a nucleus/matrix interface, ς is a correction factor for the surface energy of an interface connected with the presence of dislocations and having a value between 0 and 1, and ΔG_{chem} and ΔG_{ε} are the changes of the chemical free energy and the free energy of stresses at the formation of one formula unit of a new phase.

In simulation of nucleation the main problem is usually connected with the difficulty to evaluate the energy of stresses and the nucleus/matrix interface specific surface energy. Liu and Jonas [95, 96] suggested the way to avoid these difficulties in a case when precipitates have the same crystal structure and orientation as the matrix, but another lattice period. The consideration was accomplished by an example of nucleation of titanium carbides and carbonitrides in austenite. It was shown that the nucleus/matrix surface for the TiC critical sized nucleus is of dislocation and semi-coherent nature. In that case both σ_n and ΔG_{ε} associated with the semi-coherent interface can be described in terms of a critical coherency loss parameter C^*. This parameter is defined as a fraction of the lattice mismatch relaxed by the presence of the interface dislocations, and it can be determined directly from ΔG_{chem}.

Let us consider a general case of carbide or nitride nucleation in austenite for cubic carbides or nitrides MX_n of IV–V groups. All these carbides and nitrides have similar crystal lattices with close parameters. That's why it seems valid to extend the approach developed by Liu and Jonas [95, 96] to this case of vanadium carbides.

The Gibbs energy change at the formation of one formula unit of MX_n from austenite was calculated from:

$$\Delta G_{ch} = \frac{1}{\upsilon_{MX_n}}\left[G_{MX_n} - \overline{G}_M - n\overline{G}_X\right],$$

(88)

where G_{MX_n} and υ_{MX_n} are the Gibbs energy and volume of one MX$_n$ formula unit, respectively.

In calculation of ΔG_ε and σ_n it was assumed that δ (the lattice mismatch) is compensated by two components, elastic, δ_ε, and plastic, δ_p, both of them being associated with interface dislocations, and thus

$$\delta = \delta_e + \delta_p. \tag{89}$$

Here

$$\delta = \frac{a_{MX} - a_\gamma}{a_\gamma}, \tag{90}$$

where a_{MX_n} and a_γ are the MX$_n$ and austenite lattice periods.

A coherence loss parameter is defined as

$$C^* = \delta_P/\delta. \tag{91}$$

From (89) and (91) we get

$$\delta_\varepsilon = (1 - C^*)\delta. \tag{92}$$

ΔG_ε is calculated from the formula by Eshelby [97]:

$$\Delta G_\varepsilon = \frac{2}{3}\mu_\gamma(\Delta^*)^2 \frac{\alpha}{\alpha + (1 - \alpha)K_\gamma/K_{MX_n}}, \tag{93}$$

where

$$\Delta^* = \delta_\varepsilon^3 + 3\delta_\varepsilon^2 + 3\delta_\varepsilon, \tag{94}$$

$$K_\gamma = \mu_\gamma\left[2 + 3/(1 - v_\gamma)\right], \tag{95}$$

$$K_{MX_n} = \mu_{MX_n}[2 + 3/(1 - v_{MX_n})] \tag{96}$$

$$\alpha = (1 + v_\gamma)/3(1 - v_\gamma). \tag{97}$$

Here μ_γ and μ_{MX_n} are the shear modules, and v_γ and v_{MX_n} are Poisson coefficients of the austenite and the vanadium carbide, respectively.

Similar to Liu and Jonas [95, 96], the free energy of a semi-coherent nucleus/matrix interface was considered as consisting of two parts and expressed as:

$$\sigma_n = \sigma_{nc}(1 - 2C^*\delta) + \sigma_{ns}, \tag{98}$$

where σ_{nc} corresponds to the energy of a completely coherent interface, and σ_{ns} is connected with boundary dislocation energy.

According to Liu and Jonas [95, 96], these constituents of the free energy of a nucleus/matrix interface may be expressed as follows:

$$\sigma_{nc} = \left[N_s Z_s \left(\overline{X}_M - {}^{MX_n}X_M \right)^2 \Delta H \right] / (N_A Z) \tag{99}$$

and

$$\sigma_{ns} = \left(\mu^* a^* / 2\pi^2 \right) \left[1 + \Psi - \left(1 + \Psi^2 \right)^{1/2} \right], \tag{100}$$

where

$$\Psi = 2\pi a^* / [\lambda(1 - v^*)] \tag{101}$$

and

$$\lambda = a^*/\delta_p = a^*/C^*\delta. \tag{102}$$

Here N_S is the number of atoms per an interface surface unit, Z_s is the number of bonds through an interface per atom, N_A is the Avogadro number, Z is a coordinate number, ΔH is the enthalpy of the vanadium carbide dissolution in the infinitely diluted austenite, a^* is the interfacial lattice parameter defined as $a^* = 2a_\gamma a_{MX_n} / \left(a_\gamma + a_{MX_n} \right)$, μ^* is the interfacial shear modulus, and v^* is the interfacial Poisson's ratio.

Following Van der Merve [98], the values of μ^* and v^* can be evaluated from the precipitate and matrix shear modules and Poisson's ratios:

$$1/\mu^* = 1/\mu_\gamma + 1/\mu_{MX_n} \tag{103}$$

and

$$1/v^* = 1/v_\gamma + 1/v_{MX_n}. \tag{104}$$

It is obvious from the above derivations that both ΔG_ε and σ_n are the functions of C^*. To determine C^* we used the expression by Liu and Jonas [95, 96]:

$$(\sigma_n/\sigma_0)^{1.5} = 1 + \Delta G_\varepsilon / \Delta G_{ch}, \tag{105}$$

where σ_0 is the energy of a non-coherent precipitate/matrix interface.

Substitution of (88–104) expressions into (105) gives an equation with one unknown, which can be numerically calculated to determine C^* and then calculate ΔG_ε and σ_n.

The calculation procedure is in many respects similar to that described above and used in [89, 91, 92]. However, in the case considered the nucleation is taken into account along with the processes of precipitate growth and dissolution.

The calculation procedure is as follows:

1. Calculation of average component concentrations in the matrix based on the precipitate volume fraction.
2. Calculation of the field cell sizes.
3. Construction of spatial nets in field cells of all size intervals.

4. Calculation of concentration distributions in cells and interface velocities for particles of different size intervals.
5. Calculation of the nucleation rate.
6. Calculation of the PSDs and volume fraction at a new time step without regard for nucleation processes.
7. Calculation of the volume fraction and the PSD with consideration for the formation of new nuclei.
8. The as-determined values of the volume fraction and the PSDs were used as the initial ones for calculations at a new time step, and so on. This procedure is repeated until the necessary time is reached.

Points I–IV are completely similar to the above described steps of calculation of precipitates evolution without considering nucleation.

The nucleation rate (J) and the critical nucleus radius (R_{crit}) were calculated at every time step as follows. These parameters were calculated based on the mean component concentrations in a matrix, i.e. without considering the non-uniformity of the component concentration distribution, in particular, its decrease near the growing particles. Based on the values of the average component concentrations in matrix, the change of the chemical free energy at the formation of one formula unit of a new phase was calculated from equation (88). A critical coherency loss parameter C^* was then calculated from Eq. (105) in view of equations (88–104). From the value of this parameter the ΔG_ε and σ_n were calculated using Eqs. (93) and (98). After that the free energy of the critical nucleus formation and the nucleation rate were calculated from Eqs. (90) and (89), respectively.

Calculations of the PSD and the particle volume fraction at a new time step without regard for the precipitate nucleation were performed as described in the above section.

The volume fraction and PSD calculations corrected for the formation of new nuclei were performed as follows. The number of nuclei forming in a unit volume during the Δt time was calculated from the nucleation rate:

$$N_n = J \cdot \Delta t \tag{106}$$

The increase of the precipitates volume fraction due to the formation of new nuclei was calculated from the formula:

$$\Delta F = \frac{4\pi}{3} R_{crit}^3 \cdot N_n \tag{107}$$

The PSD change due to the formation of new nuclei was calculated based on the following considerations. The nucleation results in the growth of the fraction of particles in the size interval where the critical sized particles fall, and this growth is calculated from:

$$\Delta n_{crit.} = \frac{N_n}{N_p}, \tag{108}$$

where $\Delta n_{crit.}$ is the change of particle fraction in a size interval where the critical sized particles fall; and N_p is the total amount of particles in a volume unit before the formation of new nuclei, the latter being calculated from:

$$N_p = \frac{3F}{4\pi\overline{R}^3}, \tag{109}$$

where $\overline{R}$ is the average precipitate radius.

After the introduction of this correction the PSD was normalized. Using the algorithm developed we carried out calculations of the vanadium carbide precipitates evolution in an austenite matrix [99, 100]. Based on the results of the experimental investigations by Jack and Jack [101] and the thermodynamic analysis by Popov et. al. [102], the mean composition of the carbides in a steel was assumed to correspond to $VC_{0.88}$.

In [99] the calculation results were compared to the experimental data by Wey et. al. [69], who investigated vanadium carbide evolution in the austenite of steel with 1.1 wt. % of vanadium and 0.86 wt. % of C. The heat treatment was as follows. The samples were water quenched from 1,300 °C, then heated up to 700 °C and held for 5 h at this temperature for the formation of the dispersed precipitates, and finally annealed at 900–1,100 °C from 10 to 200 h. Wey et. al. [69] investigated the changes of mean precipitate size and PSD in the process of the final heat treatment. As regards the state of these precipitates after the 5 h annealing at 700 °C considered as the initial one for the subsequent treatment, it was not studied. That is why it was necessary to set the particles size distribution and their volume fraction in the initial state, required for further calculations, using some assumptions.

Based on the analysis of a number of publications including those by Dunlop and Honeycombe [103] and Ballinger and Honeycombe [104], we assumed the average carbide particle radius to be about 30 nm. The PSD was assumed to be normal with the standard deviation of about 0.3. By all means such a choice of these parameters implies a considerable error in their values, but in the case under consideration it doesn't remarkably affect the calculation results.

The volume fraction value in the initial state was chosen reasoning from the following considerations. There are two different sections in the experimental dependences of the precipitate cubed average radius on the annealing times presented by Wey et al. [69]. In the first section the rate of precipitate growth is relatively high and the R^3 dependence on the annealing time is non-linear. The diffusion growth of precipitates is assumed to proceed at this stage through the vanadium and carbon transition from the solid solution into the particles. In the second section the $\overline{R}^3$ dependence is nearly linear suggesting the coarsening to occur. In the stage of coarsening the precipitate volume fraction is near to its equilibrium value. At 1,100 °C the solid solution supersaturation is relatively low, and thus the formation of new nuclei is unlikely. It is therefore possible to determine the carbide volume fraction in the initial state analysing the temporal
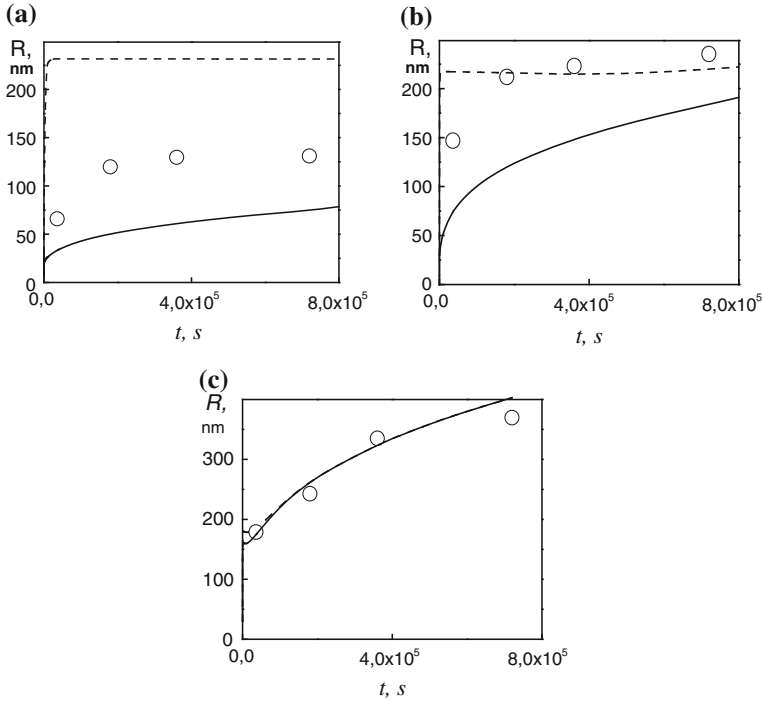
Fig. 24 VC$_{0.88}$ average radius dependence on the annealing time at 900 (**a**), 1,000 (**b**) and 1,100 °C (**c**): *dashed lines*—calculation without regard for nucleation, *solid lines*—calculation with regard for nucleation, spheres—experimental data by Wey et. al. [69]

dependence of the precipitate cubed average radius at this temperature. If there is no nucleation of precipitates, then the ratio of the cubed average radiuses of precipitates in the initial state and in the moment of growth stage completion (the beginning of the coarsening stage) is equal to the ratio of their volume fraction in the initial state to the equilibrium volume fraction. If the equilibrium volume fraction is known (and it was assessed based on the thermodynamic calculation), then it is possible to estimate the precipitate volume fraction in the initial state. This assessment gives the value of 0.000046.

The comparison of calculation results to the experimental data was performed for 900, 1,000 and 1,100 °C annealing for up to 200 h. The experimental data were compared to the calculation results obtained both with consideration for nucleation and without it.

Figure 24 demonstrates calculated and experimental dependences of the precipitate average radii on the annealing time at 900, 1,000 and 1,100 °C, and Figs. 25, 26, 27 show calculated and experimental PSDs after the annealing at these temperatures for 10, 50, 100 and 200 h. The Lifshitz–Slezov's asymptotic distribution is shown for the comparison by a dotted line.
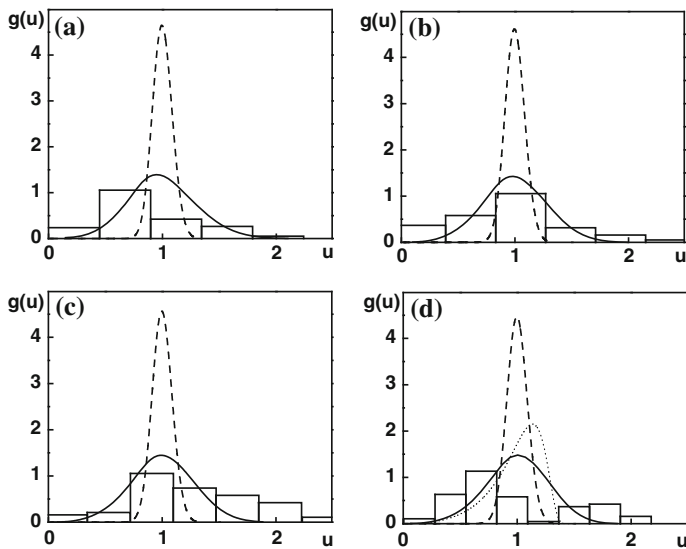
Fig. 25 Calculated and experimental VC$_{0.88}$ PSDs after 900 °C annealing for 10 (**a**), 50 (**b**), 100 (**c**) and 200 h (**d**): histograms—experimental data by Wey et al. [69], *dashed lines*—calculation without regard for nucleation, *solid lines*—calculation with consideration for nucleation, *dotted line*—asymptotic Lifshitz-Slezov's PSD

Fig. 26 Calculated and experimental VC$_{0.88}$ PSD after 1,000 °C annealing for 10 (**a**), 50 (**b**), 100 (**c**) and 200 h (**d**): histograms—experimental data by Wey et al. [69], *dashed lines*—calculation without regard for nucleation, *solid lines*—calculation with consideration for nucleation, *dotted line*—asymptotic Lifshitz-Slezov's PSD
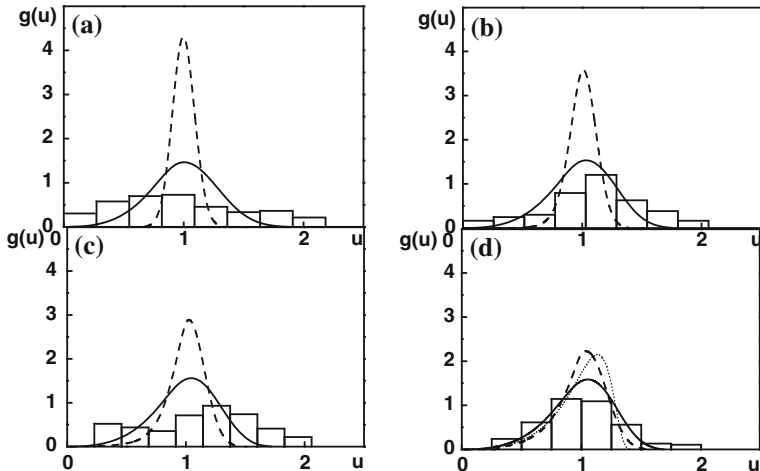
Fig. 27 Calculated and experimental VC$_{0.88}$ PSD after 1,100 °C annealing for 10 (**a**), 50 (**b**), 100 (**c**) and 200 h (**d**): histograms—experimental data by Wey et al. [69], *dashed lines*—calculation without regard for nucleation, *solid lines*—calculation with consideration for nucleation, *dotted line*—asymptotic Lifshitz-Slezov's PSD
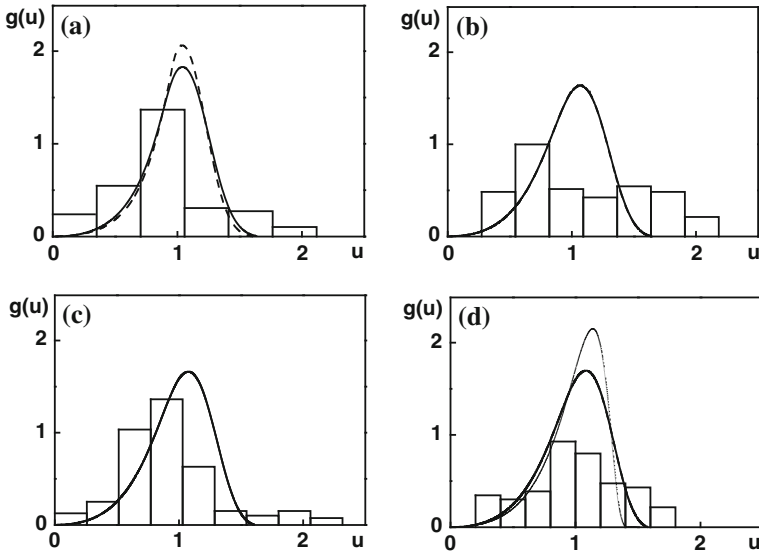
It can be seen that according to the calculation results without considering nucleation there are three stages on the temporal dependence of the average particle radii. At first the fast growth of particles occurs due to vanadium and carbon transfer from a supersaturated solid solution into precipitates, resulting in a quick increase of their average radius. Quite a narrow PSD is forming at this stage. Then the stage of particle size stabilization comes, their average radii practically not changing. This stage results from the formation of a very narrow PSD in the process of precipitate growth. As the element concentrations at interfaces with different particles are practically the same, the coarsening is not possible in that case. That is why the average radius practically does not change, and only the PSD changes. With the growth of the PSD width the coarsening stage begins. The duration of every stage depends on the annealing temperature. At 900 °C the narrow PSD forming in the process of particle growth is very stable, and the coarsening stage does not occur even after the 200 h annealing. At 1,000 °C the PSD broadens markedly, and the coarsening stage begins after the 100 h annealing. And, finally, at 1,100 °C the narrow PSD, forming at the initial stage, broadens already after the 10 h holding, and the coarsening stage is observed.

The comparison of calculations without considering nucleation with the experimental data demonstrates their good agreement only at 1,100 °C. At lower temperatures the calculation and experimental results considerably differ. The main difference is that the calculation predicts a very fast growth of the particle

average radius and the formation of a very narrow PSD resulting in the particle size stabilization, which does not agree with the experiment. Firstly, at the initial stage the particle radius growth is not as fast and the PSD is not as narrow, as it is predicted by calculations. Secondly, the stage of the particle size stabilization is not observed on the experimental dependences of the particle average radius.

If calculations are performed with consideration for nucleation, they are much closer to the experiment. In that case the particle average radius dependences on the annealing time are not so steep, there is no stabilization stage in them, and the calculated PSDs are wider and closer to the experimental ones. Such an effect of nucleation may be explained as follows. At the first stage, when the particles present in the initial state are growing, the nucleation results in a slower increase of the particle average radius because of high dispersity of the new forming particles. For the same reason a relatively broad particle size distribution is forming at the initial stage of the process, when the growth of the particles present is accompanied by nucleation of the new ones. Thus, in calculations taking nucleation into account the particle growth together with the formation of new nuclei is right away followed by coarsening, missing the stabilization stage, which was found in calculations without regard for nucleation.

The greatest difference between calculations with and without considering nucleation is typical of the 900 °C annealing, as at this temperature the solid solution in the initial stage is highly supersaturated, and the intensive nucleation occurs. At 1,100 °C it is only slightly supersaturated, and nucleation is not well developed. As a result, in this case the calculation results with and without considering nucleation are quite close to each other, and while there are slight differences after 10 h annealing, at longer holding the average radiuses and PSDs are practically the same. The longer is the holding and the higher is the annealing temperature, the closer is the calculated distribution to the Lifshitz-Slezov's asymptotic curve.

The analysis of the results obtained demonstrates satisfactory agreement of calculations considering nucleation with the experimental data. The discrepancies observed result from several reasons. Firstly, it is the absence of any experimental data on the volume fraction and the particle size distribution at the initial stage, which made it necessary to choose these parameters quite arbitrarily. Secondly, there is no information on dislocation density and its changes at annealing. Thirdly, there exist some errors in the values of parameters used in calculations. We suppose that these factors are mainly the reasons of the discrepancies observed, but not the imperfectness of the model suggested.
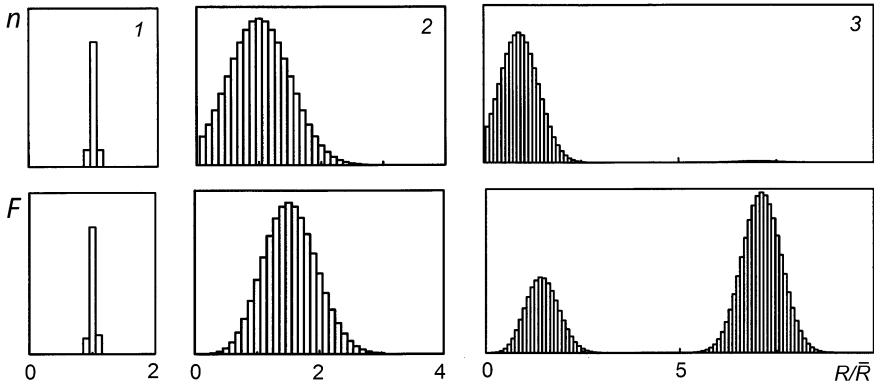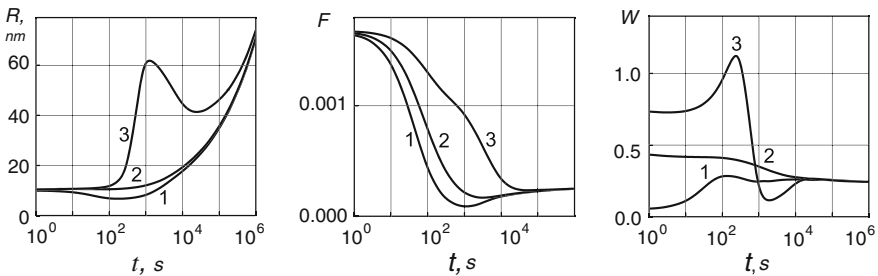
Fig. 28 Three types of the initial PSDs

Fig. 29 Variation of $VC_{0.88}$ average radius (R), volume fraction (F) and PSD width (W) at 900 °C annealing of steel with 1 % C and 0.1 % V: $R_0 = 10$ nm, $F_0 = 0.0017$. Figures near *curves* denote the type of the initial PSD

4.4 Effect of the Initial Particle Size Distribution on Precipitate Evolution

Using the algorithm developed, the influence of the initial PSD on further precipitate evolution has been analyzed, the analysis having shown the strong dependence of particles ensemble evolution on the initial PSD [10, 100]. To illustrate that we present here the calculation results of simulation of vanadium carbides growth and dissolution in austenite for three initial PSDs [100]:

1. A very narrow PSD (the width of 0.5 nm) given by a normal distribution with the center at 10 nm.
2. A relatively wide PSD (the width of 5 nm) given by a normal distribution with the center at 10 nm.

3. A bimodal PSD, given by a sum of two normal distributions the width of 5 nm with the centers at 9 and 70 nm. The volume fraction of particles corresponding to them was 0.99 and 0.01 respectively.

The average particle size for all the three types of PSDs was the same, 10 nm. Figure 28 demonstrates the normalized histograms of the initial PSDs, the upper ones for every PSD showing the number of particles (n), and the lower ones—the volume fraction of particles (F) corresponding to every size interval. The latter histograms show how the precipitates volume is distributed between the particles of different sizes.

Figure 29 demonstrates dependences of VC average size, their volume fraction and PSD width on the annealing time at 900 °C for steel with 0.1 wt. % V and 1.0 wt. % C. The volume fraction of the precipitating phase was 0.0017 in the initial state, which corresponded to the maximal possible amount of VC in the steel of composition considered and was substantially more than the equilibrium value. At heating of this steel up to 900 °C precipitates at first partly dissolve, and then the coarsening stage starts. At the dissolution stage the free energy of a system decreases mainly at the expense of its volume constituent through the reduction of the precipitate volume fraction. When phase composition approaches its equilibrium value, the coarsening stage starts.

At the dissolution stage the precipitates volume fraction reduces which is accompanied with particle size changes. In that case the initial PSD has a strong effect on precipitates average size and volume fraction temporal dependences.

In case of a narrow initial PSD (type 1) the dissolution is the most rapid process and it is accompanied with the decrease of the precipitate average size. The precipitates dissolution results in the reduction of their volume fraction up to the value lower than the equilibrium one. This is due to the fact that in that case particles become highly dispersed, and that is why their solubility increases.

Precipitate dissolution is accompanied by a noticeable grow of the PSD width, which may be explained as follows. Fine particles dissolve faster than the coarse ones, and, consequently, the narrow initial PSD substantially broadens.

In case of wide initial PSD (type 2) dissolution proceeds slower because in that case the main precipitate volume is concentrated in coarser particles, which dissolve slower. In spite of dissolution, the average particles size at first does not change and at later stages even grows, because at dissolution not only particle sizes reduce, but the most dispersed particles completely disappear. The PSD width at precipitate dissolution in this case changes only slightly.

The dissolution is the slowest in case of the bimodal PSD (type 3). The most complicated dependences of the average size, volume fraction and PSD width on the annealing time are characteristic of this case. For understanding of these dependences one should remember that coarse particles dissolve much slower than small ones. At first small particles dissolve, while the coarse particles only slightly reduce in sizes. The complete dissolution of fine particles results in the several times growth of the average size. At further annealing the precipitate average size slightly reduces due to their dissolution. After the complete dissolution of fine
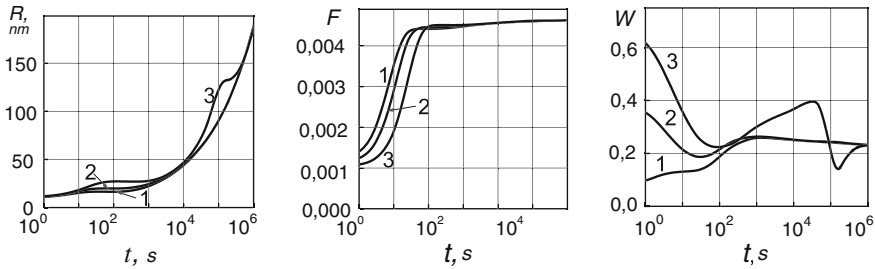
Fig. 30 VC particles average size (R), their volume fraction (F) and PSD width (W) in steel with 1 % C and 0.5 % V versus the annealing time at 1,000 °C: $R_0 = 10$ nm, $F_0 = 0.001$. Figures near *curves* denote the type of the initial PSD

particles the process slows down, and a fold appears on the volume fracture temporal dependences. The PSD width at the step of fine particles dissolution at first increases due to the broadening of the initial distribution, and then drastically reduces at their full dissolution, and the distribution is no more bimodal. At further dissolution of coarse particles the PSD width grows again.

After dissolution the coarsening stage comes, at which the particles volume fracture is close to the equilibrium and only slightly changes with time, the cube of the average size linearly depends on time and the distribution width tends to an asymptotic value. At the coarsening stage the curves corresponding to different initial distributions flow together.

To illustrate the initial PSD influence on the particles growth kinetics the precipitate evolution in steel with 0.5 % V and 1.0 % C at 1,000 °C has been simulated. The volume fracture of VC particles in the original state was taken 0.001, which is several times lower than the equilibrium value (0.00463). Figure 30 demonstrates the calculation results for three initial distributions. It can be seen that there are several sections corresponding to different stages of precipitate ensemble evolution in the curves presented. The first stage corresponds to the diffusion growth of precipitates, then some intermediate stage is observed and, finally, the coarsening stage starts. The solid solution supersaturation in the initial state is not great in this case, and that is why the new nucleation centers formation is not well developed

At the stage of growth the precipitates volume fraction rapidly increases practically achieving the equilibrium value. The phase transformation is the rapidest in case of narrow PSD (type 1), and the slowest at bimodal PSD (type 3). It is explained by the fact that the greater is the interface area, the faster is the phase transformation. This area is the greatest at PSD 1, when all particles are small, and the smallest at PSD 3, when more than a half of precipitates volume fraction is concentrated in coarse particles.

At PSD 2 and 3 they, just on the contrary, get substantially narrower. Thus, the precipitate diffusion growth, if it is not accompanied by noticeable nucleation,

promotes the formation of quite narrow PSD, which is due to the fact that fine precipitates grow faster than the coarse ones.

As the solute precipitates from the solid solution, and the precipitate volume fraction approaches to its equilibrium state, the possibilities for further decrease of the system's volume free energy are exhausted, the diffusion growth ceases and the following stage of the process starts. In the examples considered the stage of particle sizes stabilization set up after the end of the diffusion growth. By the beginning of this stage a narrow PSD has been formed as a result of the previous diffusion growth, and the precipitate volume fraction attains the value close to the equilibrium one and practically does not change at further annealing.

When the distribution width attains a certain value (W $\sim$ 0.21–0.22) the precipitate ensemble average size is capable to grow by dissolution of fine and growth of coarse particles, i.e. transition to the coarsening stage occurs.

In cases 1 and 2 the PSD is close to the universal Lifshitz-Slezov's distribution [13], and at further evolution the cube of the average particles size linearly changes with time, and PSD asymptotically approaches to the Lifshitz-Slezov's one.

In case of the initial PSD 3 the evolution at the coarsening stage substantially differs, as the particles are concentrated in two appreciably differing size intervals. At coarsening particles from large size interval grow at the expense of the small ones, and the average size grows with time faster than in cases 1 and 2. At the beginning of this stage the fraction of large size particles is small, and the main part of precipitates is concentrated in the interval of small sizes. As coarsening proceeds the number of particles in the small size interval decreases. This results at first in PSD broadening, but then, at full dissolution of fine particles, in its drastic narrowing. In that case the second interval of particles size stabilization is observed, at which the narrow PSD broadens and classical coarsening starts.

At certain isothermal annealing duration the average precipitate size dependences on time for the three initial distributions flow together.

5 Simulation of Precipitate Evolution in Multiphase Systems

Simulation of evolution in multiphase systems is much poorer developed than for two-phase systems. One of the examples is publication [8], in which such simulation was made using an approach developed in [5, 6] and the MatCalc program [7]. The weakness of these publications is that the diffusion interaction of elements in matrix is not taken into account, as well as the final volume fraction of precipitates (i.e. the diffusion fields of different precipitates don't overlap). It is an essential drawback, as these two factors in some cases may considerably affect the precipitate evolution kinetics.

An approach described in the previous section is more universal compared to those realized in other studies, for instance, in [5–8] and in DICTRA program

[105]. Recently the possibility of simulation of precipitate evolution in multiphase systems was realized in the framework of this approach [106]. The model used in this case is in many respects analogous to that used for two-phase systems. As in the latter, it is assumed that all precipitates have spherical shape, the local thermodynamic equilibrium is established at interphase boundaries and mass transfer is realized by volume diffusion in matrix. The initial conditions of the problem are alloy composition and precipitating phase compositions, as well as the volume fractions (F_f) and particle size distributions at the initial moment for every phase f. The particle size distribution for every phase f is given by its own histogram, i.e., for the particles of every type, the j-th interval of their radii from $^fR_j - \Delta^f R_j/2$ to $^fR_j + \Delta^f R_j/2$ is associated with the particle fraction $^f n_j$ of this phase falling in this interval. Here ^fR_j is the average radius of particles of the j-th size interval, and $\Delta^f R_j$ is the width of the size interval for the particles of this phase.

As mentioned above, this method is based on the mean field approach. In this case the velocity of particle growth for every size interval of every phase is formulated through interaction of this particle and its mean surroundings, i.e., the interaction between particle and matrix in field cells is considered, and it is assumed that component concentrations at all cell boundaries are the same:

$$^{fj}C_i^m\left(r = {}^fR_j^L\right) = C_i^L, \tag{110}$$

where $^{fj}C_i^m$ is concentration of the i-th component in the matrix cell connected with the particle of phase f in the j-th size interval, $^mC_i^L$ is concentration of the i-th component in matrix at cell boundaries, r is a spatial coordinate, and $^fR_j^L$ is the field cell radius connected with a particle of phase f in the j-the size interval.

To find field cell sizes, the same models were used as in case of binary systems. We used the model suggested in [70]. In case of a multiphase system, Eq. (59) takes the form:

$$^fR_j^L = {}^fR_j \cdot \left(\sum_f F_f\right)^{-1/3}. \tag{111}$$

As in the previous cases, the step-by-step procedure was used in calculations, and based on precipitate volume fraction and PSD for time t these parameters were calculated for $(t + \Delta t)$. The system of diffusion equations describing diffusion in a cell connected with a particle of phase f from the j-th size interval for a $(N + 1)$-component system is:

$$\frac{\partial^{fj}C_i^m}{\partial \tau} = \frac{1}{r^2}\frac{\partial}{\partial r}\left(r^2 \cdot \sum_{l=1}^N \widetilde{D}_{il}\frac{\partial^{fj}C_l^m}{\partial r}\right), \tag{112}$$

where $\widetilde{D}_{il}$ are partial interdiffusion coefficients in matrix.

The stationary field approach was used to find concentration distributions of elements in field cells. In this case Eq. (112) take the form:

$$\sum_{l=1}^{N} \widetilde{D}_{il} \frac{\partial^{fj} C_l^m}{\partial r} = \frac{K_i^{fj}}{r^2}, \tag{113}$$

where K_i^{fj} is a constant for the i-th element in a cell of the j-th size interval for precipitates of phase f.

As mentioned above, component concentrations at interphase boundaries must satisfy the local equilibrium and mass balance conditions.

The mass balance conditions at an interphase boundary for precipitates of phase f from the j-th size interval are:

$$\left[C_i^f v_a^m / v_a^f - {}^j C_i^{m/f} \right] \frac{dR_j}{dt} - \sum_{l=1}^{N} \widetilde{D}_{il} \frac{\partial^{fj} C_l^m}{\partial r} = 0, \tag{114}$$

or, taking into account (113):

$$\left[C_i^f v_a^m / v_a^f - {}^j C_i^{m/f} \right] \frac{dR_j}{dt} - \frac{K_i^{fj}}{\left({}^f R_j \right)^2} = 0, \tag{115}$$

where ${}^j C_i^{m/f}$ is the concentration of the i-th element in matrix at an interface with particles of phase f from the j-th size interval.

As in the above considered cases, the system of equations, satisfying the component concentration distributions in field cells and interface velocities, should be supplemented by the mass conservation condition. In this case the latter is (for every element i):

$$\Phi_i = \sum_f \alpha_f \, C_i^f + \left(1 - \sum_f \alpha_f \right) \overline{C}_i^m - C_i^{al} = 0. \tag{116}$$

The general calculation procedure used in this algorithm is in many respects analogous to those described above. As in the previous cases, the step-by-step procedure was used in calculations. The finite difference method was used for calculation of component concentrations in cells. At every step spatial nets were constructed for field cells of all phases and all size intervals. Concentration distributions in cells and interface velocities were calculated with the requirement that the average component concentrations in matrix satisfy the mass conservation condition. The local equilibrium and mass balance conditions at interfaces for all phases and all size intervals must be fulfilled, and component concentrations at cell boundaries of all size intervals must be the same.

When the interface velocities have been found, the volume fractions and PSDs for all phases at a new time step are calculated.

In [106] this algorithm was used for calculation of precipitate evolution in steels with Ti and Nb, in which two carbonitride phases are formed, one of them based on Ti nitride and another one based on Nb carbide. The calculation was performed for steel with 0.1 wt. % C, 0.01 wt. % N, 0.05 wt. % Nb and 0.03 wt. % Ti. As an example, we consider a case when the initial state was an equilibrium phase
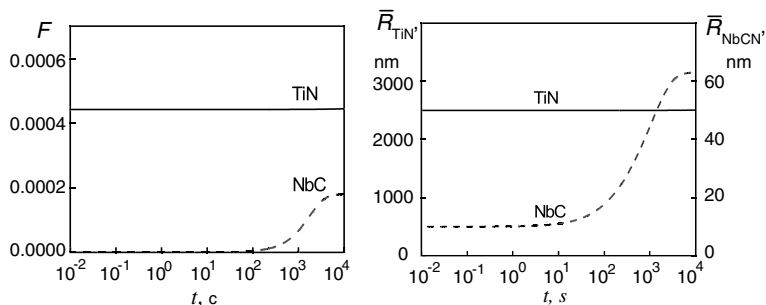
Fig. 31 Volume fraction (F) and precipitate average radius ($\bar{R}$) in the alloy with 0.1 wt. % C, 0.01 wt. % N, 0.05 wt. % Nb and 0.03 wt. % Ti versus annealing time at 1,100 °C

composition at 1,400 °C, which is close to the alloy state directly after crystallization. At this temperature the volume fraction of TiN is 0.044 %. As an initial volume fraction of NbC for further simulation the value of 0.0001 % was taken. The average radius of TiN particles was assumed to be 2.5 μm, and that of NbC 10 nm. PSDs for both phases were given by normal distributions with relative width of 0.2. Precipitate evolution in this alloy was calculated for 1,100 °C, and the results are shown in Fig. 31.

It is seen that at annealing the state of the ensemble of practically insoluble in solid steel titanium nitrides almost does not change, whereas the average radius and volume fraction of niobium carbides are considerably increased.

6 Conclusions

In recent years considerable progress has been achieved in simulation of precipitate reactions in metal alloys and of precipitate behavior at heat treatment due to the following reasons. Firstly, accumulation of experimental information has made it possible to develop physically justified models of such processes. Secondly, the development of highly-productive machine-computing technique has made it possible to carry out calculations based on complicated physical models, adequately describing the real processes. Thirdly, reliable data on thermodynamic, diffusion and other parameters required for such calculations in real metal alloys have appeared.

In this chapter the possibilities of simulation of precipitate evolution at heat treatment are demonstrated by an example of Fe-based alloys. The main attention is paid to an approach developed in the author's works and based on the mean field approximation. It is demonstrated that in this case it is possible to simulate various stages of precipitate evolution in multicomponent multiphase systems in the framework of the unified approach.

However it should be noted that there is a number of reasons which retard carrying out practical kinetic calculations for concrete alloys. First of all, one should mention the lack of the required data, such as diffusion parameters required for the description of diffusion processes in multicomponent systems. There is even poorer information on the energy of precipitate/matrix interfaces and the values of elastic constants for temperatures at which heat treatments of steels are usually carried out. The models of heterogeneous nucleation of precipitates in multicomponent alloys are also quite poorly developed. All these factors make it necessary to use various simplifications and assumptions in calculations.

The use of simplifications and assumptions is the main reason of discrepancies between calculations and experimental data. To overcome this difficulty, more perfect models of precipitate evolution should be developed, and such work is in progress now. However, for practical kinetic calculations much experimental work is also required to overcome the deficiency of various parameters necessary for calculations.

References

1. Wang, Y., Banerjee, D., Su, C.C., Khachaturian, A.G.: Field kinetic model and computer simulation of precipitation of L12 ordered intermetallics from FCC solid solution. Acta Mater. **46**, 2983–3001 (1998)
2. Snyder, V.A., Alkemper, J., Voorhees, P.W.: Transient Ostwald ripening and the disagreement between steady-state coarsening theory and experiment. Acta Mater. **49**, 699–709 (2001)
3. Vaithyanathan, V., Chen, L.Q.: Coarsening of ordered intermetallic precipitates with coherency stress. Acta Mater. **50**, 4061–4073 (2002)
4. Fujita, N., Bhadeshia, H.K.D.H., Kikuchi, M.: Precipitation sequence in niobium-alloyed ferritic stainless steel. Model. Simul. Mater. Sci. Eng. **12**, 273–284 (2004)
5. Svoboda, J., Fischer, F.D., Fratzl, P., Kozeschnik, E.: Modelling of kinetics in multi-component multi-phase systems with spherical precipitates I: Theory. Mater. Sci. Eng., A **385**, 166–174 (2004)
6. Kozeschnik, E., Svoboda, J., Fratzl, P., Fischer, F.D.: Modelling of kinetics in multi-component multi-phase systems with spherical precipitates II: Numerical solution and application. Mater. Sci. Eng., A **385**, 157–165 (2004)
7. Kozeschnik, E., Svoboda, J., Fischer, F.D.: Modified evolution equations for the precipitation kinetics of complex phases in multi-component systems. CALPHAD. **28**, 379–382 (2004)
8. Srinivas Prasad, B.S., Rajkumar, V.B., Hari Kumar, K.C.: Numerical simulation of precipitate evolution in ferritic–martensitic power plant steels. CALPHAD. **36**, 1–7 (2012)
9. Rubinshtein, L.I.: Stephan's problem, p. 238. Zvaigzne, USSR, Riga (1967). (in Russian)
10. Popov, V.V.: Simulation of carbonitride transformations at heat treatment of steels, p. 380. Ural Branch of RAS, Russia, Ekaterinburg (2003). (in Russian)
11. Hillert, M., Agren, J.: Diffusional transformations under local equilibrium. In: Embury, J.D., Purdy, GR, (ed.) Advances in phase transformations, Pergamon Press, Oxford, United Kingdom, 1–19 (1988)
12. Aaron, H.B., Fainstein, D., Kottler, R.: Diffusion-limited phase transformation: a comparison and critical evaluation of the mathematical approximation. J. Appl. Phys. **41**, 4404–4411 (1970)

13. Lyubov, B.Y., Shavelev, V.V.: Analytical calculation of kinetics of diffusion solution of another phase spherical precipitates. Fiz. Met. Metallogr. 35(2), 330–335 (1973) (in Russian)
14. Aaron, H.B., Kotler, G.R.: Second phase dissolution. Met. Trans. **2**, 393–408 (1971)
15. Lyubov, B.Y.: Diffusion processes in non-uniform solids. Moscow: Metallurgy, P. 295 (1981) (in Russian)
16. Nolfi, F.V., Shewmon, P.G., Foster, J.S.: The dissolution and growth kinetics of spherical precipitates. Trans. Met. Soc. AIME. **245**, 1427–1433 (1969)
17. Nolfi, F.V., Shewmon, P.G., Foster, J.S.: The dissolution kinetics of Fe3C in ferrite—A theory of interface migration. Met. Trans. **1**, 2291–2304 (1970)
18. Sherbedinsky, G.V., Kondrachenko, L.A.: Analysis of growth kinetics of a phase at decomposition of a triple solid solution with consideration for component interaction. Fiz. Met. Metallogr. 30(4), 685–693 (1970) (in Russian)
19. Popov, V.V., Emelyanov, D.A., Borisov, S.V.: Analytical description of multicomponent diffusion at Ti carbide dissolution in austenite. Izv. VUZov Cher. Met. 10, 94–95 (1982) (in Russian)
20. Popov, V.V., Emelyanov, D.A., Mitorfanov, B.V., Borisov, S.V.: Izv. AN SSSR Metals **5**, 112–116 (1983). (in Russian)
21. Popov, V.V., Emelyanov, D.A.: Vanadium carbide dissolution in steel in case of formation of a ferrite layer at its interface. Fiz. Met. Metallogr. 55(4), 685–692 (1983) (in Russian)
22. Voroshnin, L.G., Husid, B.M.: Diffusion mass transfer in multicomponent systems. Minsk: Hauka I Tehnika, 256 (1979) (in Russian)
23. Voroshnin, L.G., Vityaz, P.A., Hasybulin, H.G., Husid B.M.: Multicomponent diffusion in multicomponent alloys. Misk: Vyssh. Sch. p. 142 (in Russian) (1984)
24. Shatinsky, V.F., Nesterenko, A.N.: Protective diffusion coatings. Kiev: Naukova Dumka, p. 272 (in Russian) (1988)
25. Nesterenko, A.I., Nesterenko N.G.: Method of ancillary net for solution of problems with moving interphase boundaries. J. Vych. Mat. and Mat. Fiz. 24(3), 374–382 (1984) (in Russian)
26. Budack, B.M., Solovyova, E.N., Uspensky, A.B.: Difference method of Stephan's problems solution. J. Vych. Mat. and Mat. Fiz. 5(5), 828–840 (1965) (in Russian)
27. Samarcky, A.A., Moiseenko, B.D.: Economic scheme of straight-through calculation for multidimensional Stefan's problem. J. Vych. Mat. and Mat. Fiz. 5(5), 816–827 (1965) (in Russian)
28. Budack, B.M., Goldman, N.L., Egorova, A.T.: Method of fronts straightening for solution of Stefan-type problems. Vych. Meth. and Progr. Proc. MSU. 8, 103–121 (1967) (in Russian)
29. Vasiliev, F.P., Uspensky, A.B.: Difference method of two-dimensional Stephan-type problem solution. J. Vych. Mat. and Mat. Fiz. 3(5), 874–886 (1963) (in Russian)
30. Budack, B.M., Malomed, V.T.: Numerical solution of Stefan-type problem for one quasi-linear parabolic problem. Vych. Meth. and Progr. Proc. MSU. 6, 121–133 (1967) (in Russian)
31. Douglas, J., Gallie, T.: On the integration of a parabolic differential equation subject to a moving boundary condition. Duke Math. J. **55**, 557–572 (1955)
32. Volkov, S.A.: Numerical solution of two-phase Stephan's problem. Vych. Meth. and Progr. Proc. MSU. 6, 124–138 (1967) (in Russian)
33. Nesterenko, A.I., Shatinsky, V.F., Shapoval, N.N.: Kinetic assessment of durability of multiphase coatings in aggressive environments at high temperatures. Phys.-Chim. Mech. Mater. 16(5), 78–82 (1980) (in Russian)
34. Shatinsky, V.F., Nesterenko, A.I.: Problems of non-stationary mass transfer in some high-temperature technological processes. Izv. AN SSSR. Metals. 5, 41–43 (1981) (in Russian)
35. Tanzilli, R.A., Hechel, R.W.: Numerical simulations to the finite, diffusion-controlled two-phase, moving-interface problem (with planner, cylindrical and spherical interfaces). Trans Met. Soc. AIME. **242**, 2313–2321 (1968)

36. Murrey, W.D., Landis, F.: Numerical and machine solutions of transient heat-conduction problem involving melting or freezing. I. Method of analysis and sample solutions. J. Heat Transfer **84**, 106–112 (1959)
37. Agren, J.: Numerical treatment of diffusion reactions in multicomponent alloys. J. Phys. Chem. Sol. **43**, 385–391 (1982)
38. Popov, V.V., Lobanov, M.L.: Mathematical simulation of diffusion interaction of interstitial phase with solid solution in three-component system. Fiz. & Chim. Obr. Mat. (Physics and Chemistry of Materials Treatment). 4, 133–138 (1995) (in Russian)
39. Popov, V.V.: Numerical simulation of diffusion interaction of precipitates with matrix in multicomponent systems. Metals **2**, 129–138 (1997). (in Russian)
40. Popov, V.V.: Simulation of dissolution of Carbide and Nitride precipitates in Austenite. Phys. Met. Metallogr. **84**, 349–358 (1997)
41. Akimova, E.N., Gorbachev, I.I., Popov, V.V.: Solution of problems of multicomponent diffusion with parallel algorithm of matrix fitting. Mathematical Modelling **17**(9), 85–92 (2005). (in Russian)
42. Lyahovich, L.S., Voroshnin, L.G., Husid, B.M.: Diffusion mass transfer studies in multicomponent solutions. Izv. BSSR, Ser. Fiz.-Energ. Nav. 4, 116–122 (1976) (in Russian)
43. Popov, V.V.: Exceed phase dissolution in constructional steels at heat treatment. Met. and Term. Obr. Met. (Metallography and heat treatment of metals). 10, 28–32 (1995) (in Russian)
44. Lyubov, B.Ya.: Diffusion processes in inhomogeneous solids. Moscow: Metallurgy, p. 295 (1981) (in Russian)
45. Gorbachev, I.I., Popov, V.V., Akimova, E.N.: Computer simulation of the diffusion interaction between carbonitrides precipitates and austenitic matrix with allowance for the possibility of variation of their composition. Phys. Met. Metallogr. **102**(1), 18–28 (2006)
46. Popov, V., Gorbachev, I.: Simulation of precipitates evolution in steels. Defect and Diffusion Forum. **263**, 171–176 (2007)
47. van Loo, F.J.J., Bastin, G.F.: On the diffusion of carbon in titanium carbide. Metall. Trans. A **20A**(3), 403–411 (1989)
48. Levinsky, Yu.F., Stroganov, Yu.D., Salibekov, S.E., et al.: Studies of diffusion of nitrogen in titanium. Izv. AN SSSR, Neorg. Mater. 4(12), 2068–2073 (1968) (in Russian)
49. Anderson, J.-O., Agren, J.: Models for numerical treatment of multicomponent diffusion in simple phases. J. Appl. Phys. **72**, 1350–1355 (1992)
50. Meyer, L., Buhler, H.E., Heisterkamp, F.: Metallkundliche Untersuchangen zur Wirkungsweise von Titan in Unlegierten Baustahlen. Arch. Eisenhuttehw. **43**, 823–832 (1972)
51. Dergunova, V.S., Levinsky, Yu.V., Shurshakov, A.N., et al.: Carbon Interaction with Refractory Metals. In: Samsonov, G.V. Metallurgiya Publications, Moscow, Russia, (1974) (in Russian)
52. Teichmann, C., Lengauer, W., Ettmayer, P., Bauer, J., Bohn, M.: Reaction diffusion and phase equilibria in V-N system. Metall. Mater. Trans. **28A**, 837–842 (1997)
53. Lifshitz, I.M., Slezov, V.V.: On kinetics of diffusion decomposition of supersaturated solid solutions. J. Exp. & Teor. Fiz. 35, **2**(8), 479–492 (1958) (in Russian)
54. Ardell, A.A.: Interfacial free energies and solute diffusivities from data on Ostwald Ripening. Interface Sci. **3**, 119–125 (1995)
55. Wagner, C.: Theorie der Alterung von Niederschlangen durch Umlose Ostwald–Reifung. Z. Elektrochem. **65**(7–8), 581–591 (1961)
56. Slezov, V.V.: Coalescence of saturated solid solution in case of diffusion along block boundaries and dislocation lines. Fiz. Tverd. Tel. (Solid state physics). 9(4), 1187–1191 (1967) (in Russian)
57. Kreye, H.: Einflub von Versetzungen auf die Umlosung von Teilchen. Z. Metallkd. **61**, 108–112 (1970)
58. Vengrenovitch, R.D.: On the Ostwald ripening theory. Acta Metall. **32**(6), 1079–1086 (1982)

59. Slezov, V.V., Sagalovich, V.V.: Diffusive decomposition in solid solutions. Soviet Physics-Uspekhi **30**, 23–45 (1987)
60. Kondratyev, V.V., Ustyugov, Y.M.: Kinetics of decomposition of supersaturated solid solutions at various mechanisms of mass transfer. I. Coarsening stage. Phys. Met. Metallogr. **76**(5), 40–50 (1993)
61. Slesov, V.V., Sagalovich, V.V.: Theory of coarsening in multicomponent multiphase systems. Fiz. Tv. Tela (Solid State Physics). 17(5), 1497–1499 (1975) (in Russian)
62. Slesov, V.V., Sagalovich, V.V.: Coexistence regions of phases at diffusion decomposition of supersaturated multicomponent systems Fiz. Tv. Tela (Solid state physics). 17(9), 2751–2753 (1975) (in Russian)
63. Slesov, V.V., Sagalovich, V.V.: Theory of diffusive decomposition of supersaturated multicomponent systems. J. Phys. Chem. Sol. **38**, 943–948 (1977)
64. Kuehmann, C.J., Voorhees, P.W.: Ostwald ripening in ternary alloys. Metall. Mater. Trans. **27A**(4), 937–943 (1996)
65. Hoyt, J.J.: Coarsening in multiphase multicomponent systems—I, The mean field limit. Acta Mater. **47**(1), 345–351 (1999)
66. Balliger, N.K., Honeycombe, R.W.G.: Coarsening of vanadium carbide, carbonitrides and nitride in low-alloy steels. Metal Sci. **14**(4), 121–133 (1980)
67. Bjarbo, A., Hattestrand, M.: Complex carbide growth, dissolution and coarsening in a modified 12 % chromium steel—an experimental and theoretical study. Metall. Mater. Trans. **32A**(1), 19–27 (2001)
68. Atasoy, O.E.: The effect of nitrogen potential on the coarsening kinetics of VN precipitates. Metall. Trans. A **14A**(3), 379–384 (1983)
69. Wey, M.Y., Sakuma, T., Nishizava, T.: Growth of alloy carbide particles in austenite. Trans. Japan Inst. Met. **22**(10), 733–742 (1981)
70. Tsumuraya, K., Miyata, Y.: Coarsening models incorporating both diffusion geometry and volume fraction of particles. Acta Metall. **31**(3), 437–452 (1983)
71. Voorhees, P.W.: Ostwald ripening of two-phase mixtures. Ann. Rev. Mater. Sci. **22**, 197–215 (1992)
72. Ardell, A.J.: The effect of volume fraction on particle coarsening: theoretical considerations. Acta Metall. **20**, 61–71 (1972)
73. Marsh, S.P., Glicksman, M.E.: Kinetics of phase coarsening in dense systems. Acta Mater. **44**, 3761–3771 (1996)
74. Brailsford, A.D., Wynblatt, P.: The dependence of Ostwald ripening kinetics on particle volume fraction. Acta Metall. **27**, 489–497 (1979)
75. Marqusee, J.A., Ross, J.: Theory of Ostwald ripening: competitive growth and its dependence on volume fraction. J. Chem. Phys. 80, (536–543)
76. Tokuyama, M., Kawasaki, K.: Statistical-mechanical theory of coarsening of spherical droplets. Physica. **123A**, 386–411 (1984)
77. Akaiwa, N., Voorhees, P.W.: Late-stage phase separation: dynamics, spatial correlations, and structure functions. Phys. Rev. E **49**, 3860–3880 (1994)
78. Voorhees, P.W., Glicksman, M.E.: Solution to the multi-particle diffusion problem with applications to Ostwald ripening—II, Computer simulation. Acta Metall. **32**, 2013–2030 (1984)
79. Enomoto, Y., Kavasaki, K., Tokuyama, M.: Computer modelling of Ostwald ripening.: Acta Metall. 35, 907–913 (1987)
80. Mandyam, H., Glicksman, M.E.: Late-stage coarsening dynamics in phase separating systems: simulation results. Mater. Sci. Eng., A **238**, 121–127 (1997)
81. Bullard, J.W.: Numerical simulations of transient-stage Ostwald ripening and coalescence in two dimensions. Mater. Sci. Eng., A **238**, 128–139 (1997)
82. Poduri, R., Chen, L.-Q.: Computer simulation of morphological evolution and coarsening kinetics of δ' (Al3Li) precipitates in Al-Li alloys. Acta Mater. **46**, 3915–3928 (1998)
83. Voorhees, P.W., McFadden, G.B., Jonsson, W.C.: On the morphological development of second-phase particles in elastically-stressed solids. Acta Mater. **40**, 2979–2992 (1992)

84. Su, C.H., Voorhees, P.W.: The dynamics of precipitate evolution in elastically stressed solids. Acta Mater. **44**, 1987–2016 (1996)
85. Veron, M., Brechet, Y., Louchet, F.: Directional coarsening of Ni-based super alloys: computer simulation at mesoscopic level. Acta Mater. **44**, 3633–3641 (1996)
86. Popov, V.V.: Numerical simulation of the evolution of a Polydisperse ensemble of precipitates in a two-component alloy upon isothermal annealing. Phys. Met. Metallogr. **87**, 379–386 (1999)
87. Popov, V.V.: Modeling of the coalescence of γ'-phase precipitates in Ni-Si alloys. Phys. Met. Metallogr. **88**, 533–541 (1999)
88. Popov, V.V.: Simulation of growth and dissolution of γ'-phase precipitates in alloys of Ni-Si system. Phys. Met. Metallogr. **89**, 5–11 (2000)
89. Popov, V.V.: Simulation of the evolution of precipitates in dilute alloys. Phys. Met. Metallogr. **93**, 303–309 (2002)
90. Popov, V.V.: Simulation of precipitate evolution in multicomponent systems. Bull. of Cherkassy State University. **35–36**, 41–50 (2001–2002)
91. Popov, V.V.: Simulation of dissolution and coarsening of MnS precipitates in Fe-Si. Phil. Mag. A. **82**, 17–27 (2002)
92. Popov, V.V., Gorbachev, I.I.: Simulation of the evolution of precipitate in multicomponent alloys. Phys. Met. Metallogr. **95**, 417–426 (2003)
93. Asimov, R.: Clustering kinetics in binary alloys. Acta Metall. **11**, 72–73 (1963)
94. Cheng, L.M., Hawbolt, E.B., Meadowcroft, T.R.: Modeling of dissolution, growth and coarsening of aluminium nitride in low-carbon steels. Metall. Mater. Trans. A **31**, 1907–1916 (2000)
95. Liu, W.J., Jonas, J.J.: Characterization of critical nucleus/matrix interface: application to Cu-Co alloys and micro alloyed austenite. Mater. Sci. Technol. **5**(1), 8–12 (1989)
96. Liu, W.J., Jonas, J.: Nucleation kinetics of titanium carbonitride in micro alloyed austenite. Metall. Trans. A **20A**(4), 689–697 (1989)
97. Eshelby, J.D.: The determination of the elastic field of an ellipsoidal inclusion, and related problems. Proc. R. Soc. **A241**, 376–396 (1957)
98. Van Der Merwe, J.H.: Crystal interfaces. Part I. semi-infinite crystals. J. Appl. Phys. **34**, 117–122 (1963)
99. Popov, V.V., Gorbachev, I.I., Alyabieva, J.A.: Simulation of VC precipitate evolution in steels with consideration for the formation of new nuclei. Phil. Mag. A. **85**, 2449–2467 (2005)
100. Popov, V.V., Gorbachev, I.I.: Numerical simulation of carbide and nitride precipitate evolution in steels. Material wissenschaft und Werkstofftechnik **36**, 477–481 (2005)
101. Jack, D.H., Jack, K.H.: Carbides and nitrides in steel. Mater. Sci. Eng. **11**, 1–27 (1973)
102. Popov, V.V., Goldstein, M.I., Emelianov, D.F., Kostrov, U.N.: Thermodynamic calculation of solubility of cubic vanadium carbide in austenite. Izv. AN SSSR, Metals, 1, 105–109 (1986) (in Russian)
103. Dunlop, G.L., Honeycombe, R.W.K.: Ageing characteristics of VC, TiC and (V, Ti) C dispersions in ferrite. Metal Sci. **12**, 367–371 (1978)
104. Ballinger, N.K., Honeycombe, R.W.K.: Coarsening of vanadium carbide, carbonitride, and nitride in low-alloy steels. Metal Sci. **14**, 121–133 (1980)
105. Anderson, J.-O., et al.: Thermo-Calc & Dictra, Computational tools for materials science. CALPHAD **26**(2), 273–312 (2002)
106. Gorbachev, I.I., Popov, V.V., Pasynkov, A. Yu.: Simulation of precipitates evolution of two carbonitride phases in steels with Nb and Ti at isothermal annealing. Phys. Met. Metallogr. (In press) (2013)